Vascular endothelial growth factor-c regulates hematopoietic stem cell fate in the dorsal aorta

Rebecca K. Schiavo[1,2] & Owen J. Tamplin[1,2]*

[1]Department of Pharmacology, University of Illinois at Chicago, Chicago, IL 60612 USA

[2]Present address: Department of Cell and Regenerative Biology, University of Wisconsin – Madison, Madison WI 53705 USA

*Corresponding author: tamplin@wisc.edu

Keywords: VEGFC, hematopoietic stem cells, hemogenic endothelium, hematopoiesis, dorsal aorta, zebrafish

Summary statement

A novel role for vascular endothelial growth factor-c in hematopoietic stem cell fate decisions within the hemogenic endothelium.

Abstract

Hematopoietic stem and progenitor cells (HSPCs) are multipotent cells that self-renew or differentiate to establish the entire blood hierarchy. HSPCs arise from the hemogenic endothelium of the dorsal aorta (DA) during development in a process called endothelial-to-hematopoietic transition. The factors and signals that control HSPC fate decisions from the hemogenic endothelium are not fully understood. We found that *vegfc* has a role in HSPC

emergence from the zebrafish DA. Using time-lapse live imaging, we show that some HSPCs in the DA of *vegfc* loss-of-function embryos display altered cellular behavior. Instead of typical budding from the DA, emergent HSPCs exhibit crawling behavior similar to myeloid cells. This was confirmed by increased myeloid cell marker expression in the ventral wall of the DA and the caudal hematopoietic tissue. This increase in myeloid cells corresponded with a decrease in HSPCs that persisted into larval stages. Together, our data suggests *vegfc* regulates HSPC emergence in the hemogenic endothelium, in part by suppressing a myeloid cell fate. Our study provides a potential signal for modulation of HSPC fate in stem cell differentiation protocols.

Introduction

In vertebrates, hematopoiesis occurs in two waves, the primitive and definitive wave. The primitive wave occurs first, producing erythrocytes and macrophages to oxygenate and provide immune defense for the developing embryo. The definitive wave follows to produce long-term, multipotent hematopoietic stem and progenitor cells (HSPCs) that can self-renew or differentiate to create all mature blood cells. Definitive HSPCs emerge from the hemogenic endothelium (HE) in the aorta-gonad-mesonephros (AGM) region through endothelial-to-hematopoietic transition (EHT) (Müller et al., 1994, Bertrand et al., 2010, Kissa and Herbomel, 2010, Boisset et al., 2010). HSPCs then migrate to seed their intermediary niche, the fetal liver which allows for expansion of the blood stem cell pool before settling in their adult niche, the bone marrow (Ema and Nakauchi, 2000). Hematopoietic development is difficult to observe in mammals because it occurs *in utero*.

Zebrafish are an excellent alternative model organism for the study of hematopoiesis. Their external and transparent development allows for *in vivo* visualization. In zebrafish, HSPCs emerge from the HE of the dorsal aorta (DA) and migrate to their intermediary niche, the caudal hematopoietic tissue (CHT) (Murayama et al., 2006, Tamplin et al., 2015), where they expand before colonizing the adult niche in the kidney marrow (Ciau-Uitz et al., 2014). While much of the ontogeny of the hematopoietic system is conserved between mammals and zebrafish, differences exist. During mammalian emergence, HSPCs form intra-aortic hematopoietic clusters in the lumen of the DA before budding off into circulation and seeding the fetal liver (Garcia-Porrero et al., 1995, Yokomizo and Dzierzak, 2010, Boisset et al., 2010). In zebrafish, HSPCs emerge from the ventral wall of the DA and migrate through the sub-aortic space to bud into the cardinal vein (Bertrand et al., 2010, Kissa and Herbomel, 2010).

Studies in mouse have shed light on the complex fate decisions arterial endothelial cells (ECs) must progress through to become a HSPC. The initial step is specification, when a subset of ECs in the dorsal aorta begin to express hematopoietic markers Gfi1, Runx1, and Gata2, and become HE (North et al., 1999, Kobayashi-Osaki et al., 2005, Kang et al., 2018). Once the HE is specified, cells acquire expression of CD41 and c-KIT, then emerge into the lumen of the dorsal aorta to form intra-aortic hematopoietic clusters (Boisset et al., 2010). Within the clusters, cells proximal to the wall of the DA display pre-hematopoietic stem cell (HSC) type I markers (CD45-, c-KIT^{low}) and are slowly cycling, while distal cells display pre-HSC type II markers (CD45+, c-KIT^{high}) and are more proliferative (Batsivari et al., 2017, Yokomizo and Dzierzak,

2010). Distally located cells mature to become definitive HSCs, and cell cycling slows before release into circulation and migration to the fetal liver. While the process of HSPC maturation and emergence has been described, there is a lack of knowledge of factors that may influence HSPC differentiation during EHT.

Human vascular endothelial growth factor c (VEGFC) is a major driver of lymphangiogenesis through its binding to VEGF receptor-2 (VEGFR2) and VEGFR3 (Stacker et al., 2014, Joukov et al., 1996). The critical function of vegfc and its receptor flt4/vegfr3 in lymphatic development is highly conserved in zebrafish (Shin et al., 2016, Le Guen et al., 2014, Villefranc et al., 2013). Proteolytic cleavage of human VEGFC is necessary for binding to VEGFR2 and VEGFR3 (Joukov et al., 1997). The secreted proteins involved in this post-translational processing, CCBE1 and ADAMTS3, are also conserved in zebrafish, with mutants showing similar lymphatic defects (Le Guen et al., 2014, Hogan et al., 2009, Wang et al., 2020). Interestingly, recent studies have shown evolutionary differences in the binding specificity of vegfc in zebrafish (Vogrin et al., 2019). The single VEGFR2 receptor in placental mammals has two related proteins in zebrafish, kdrl and kdr, that both bind vegfa and are required for vascular development (Covassin et al., 2006, Bahary et al., 2007). In zebrafish, vegfc binds flt4/vegfr3 and kdr but not kdrl (Vogrin et al., 2019).

The role of VEGFC in hematopoiesis is still emerging and a few studies in mice have uncovered hematopoietic phenotypes. Recent studies have shown a role for Vegfc and Ccbe1 in fetal liver erythropoiesis (Fang et al., 2016, Zou et al., 2013). Ccbe1 deficient mice are anemic with impaired erythroblast proliferation and survival (Zou et al., 2013). Vegfc conditional knockout mice have decreased fetal liver erythropoiesis and overall anemia (Fang et al., 2016). After irradiation, mice lacking Vegfc showed impaired hematopoietic regeneration and delayed vascular recovery of the bone marrow niche (Fang et al., 2020). A study of embryonic day (E) 9.5 para-aortic splanchnopleural mesoderm (P-Sp) explants from *Flt4/Vegfr3* deficient mouse embryos revealed reduced hematopoietic progenitor numbers (Hamada et al., 2000). Further analysis using this P-Sp explant model demonstrated competition between Vegfa and Vegfc for binding to both Flt4/Vegfr3 and Vegfr2, resulting in synergistic regulation of hematopoietic and vascular development (Hamada et al., 2000). However, the role of VEGFC in specification of early definitive hematopoietic progenitors remains unclear.

Here, we reveal a previously unknown role for VEGFC in maintaining HSPC fate during emergence from the HE. Using time-lapse microscopy, we discovered that in zebrafish *vegfc* loss-of-function embryos there is a decrease in EHT and budding of HSPCs from the DA. We observed more cells crawling along the cardinal vein that we confirmed were myeloid cells emerging from the DA. Our findings provide insight into fate regulation during EHT that may be useful in guiding *in vitro* differentiation of HSPCs for clinical stem cell therapy.

Results

VEGFC is expressed in HSPCs and HE

Using existing gene expression datasets, we examined *VEGFC* expression in both mouse (*Vegfc*) and zebrafish (*vegfc*) HE and HSPCs. Gene expression analysis of sorted mouse hematopoietic populations shows *Vegfc* is most highly expressed in undifferentiated HSPCs (Fig. S1A) (Gazit et al., 2013, Seita et al., 2012). Single-cell RNA sequencing (scRNA-seq) of mouse DA from E9.5 to E11.5 showed *Vegfc* is expressed specifically in a population of pre-HE and HE cells (Fig. S1B,C) (Zhu et al., 2020). In zebrafish, whole-mount *in situ* hybridization (WISH) expression of *vegfc* has been observed in the DA at pre-HE (26 hours post fertilization (hpf)) and HE stages (48-72 hpf) (Gore et al., 2011, Kwon et al., 2013).

We wanted to determine the expression of *vegfc* and its receptors in EC and HSPC populations at 52 hpf so we performed scRNA-seq of sorted *flk:mCherry*+ and *cd41:gfp*+ cells, respectively, from *flk:mCherry;cd41:gfp* double transgenic embryos. Using Seurat analysis, we identified 17 unique clusters (Fig. S2). We used *myb* and *gata2b* to identify HSPC clusters, *kdrl* for ECs, and *mpx* for myeloid cells (Fig. S3A,C). As expected, HSPCs express *GFP* transcripts (*cd41:gfp*) and ECs express *mCherry* (*flk:mCherry*) (Fig. S3B). Regarding expression of *vegfc* and its receptors, *kdrl/vegfr2a* is expressed in ECs and a few HSPCs, *flt4/vegfr3* is expressed only in ECs, and *vegfc* is expressed in ECs and a subset of HSPCs (Fig. S3C). Given the conserved expression of *vegfc* in both mouse and zebrafish embryonic HSPCs, we wanted to further explore its functional role in HSPC development.

vegfc loss-of-function decreases HSPC emergence from the DA

To determine if *vegfc* plays a role in definitive hematopoiesis, we used a combination of genetic tools, including *vegfc*^{um18} null mutants (Shin et al., 2016) and a previously validated *vegfc* morpholino (MO) (Villefranc et al., 2013). We also designed CRISPR-Cas9 sgRNA to target *vegfc* in transient F0 crispants. Our sgRNA target showed 97.34% gene editing efficiency and deletions were found around the predicted cleavage site (Fig. S4A-C). We wanted to confirm that crispants and morphants displayed signs of defective lymphangiogenesis and lymphedema consistent with *vegfc*^{um18} null mutants (Shin et al., 2016). To assess lymphedema, we raised *vegfc* MO-injected and crispant-injected embryos until 5 days post fertilization (dpf) and evaluated their overall morphology. Similar to *vegfc*^{um18} null embryos, *vegfc* crispant and morphant embryos had areas of lymphedema that were not seen in control embryos (Fig. S5A,B,E,F). We examined sprouting of parachordal lymphangioblasts (PLs) in *vegfc* crispants and morphants (Fig. S5C,D,G,H), and found they had the same defects that are typical for *vegfc* mutants (Vogrin et al., 2019, Le Guen et al., 2014). We went on to use these validated genetic tools to address the function of *vegfc* in developmental hematopoiesis.

We wanted to examine HSPC formation in *vegfc* loss-of-function embryos. We looked at *cmyb* marker expression by WISH in the DA at 36 hpf and observed significantly lower expression in *vegfc* loss-of-function embryos compared to controls (Fig. S6A,B). Based on these results, we wanted to track the live dynamics of EHT in *vegfc* loss-of-function embryos. Preliminary time-lapse experiments conducted from 32 to 52 hpf revealed that HSPC production is at its highest at 48 hpf (Fig. S6C), which is consistent with previous studies (Kissa et al., 2008, Lancino et al., 2018, Kissa and Herbomel, 2010). Therefore, we performed time-lapse imaging of *flk:mCherry;cd41:gfp* embryos from 48 hpf until 52 hpf. This revealed that *vegfc* loss-

of-function embryos had significantly fewer HSPCs budding from the DA (Fig. 1A,B). HSPCs were quantified based on expression of both *flk:mCherry* and *cd41:gfp*, as well as their process of rounding up from the endothelium and budding into the cardinal vein (Fig. 1C, Movie 1). Interestingly, *vegfc* loss-of-function embryos appeared to have more cells that started to extrude from the ventral wall of the DA, as has been previously observed (Kissa and Herbomel, 2010), but they were not able to complete EHT (Fig. 1D; Movie 2). These findings were also confirmed in *vegfc* morphant embryos (Fig. S6D-F). We did not observe defective blood flow in *vegfc* loss-of-function embryos, and circulating cells are always visible (Movies 2, 4, 6, 8). Furthermore, we used the *tp1:dGFP* notch reporter line to confirm the arterial endothelium is intact in *vegfc* loss-of-function embryos prior to HSPC formation at 28 hpf (Fig. S6G). These results suggest that *vegfc* plays a role in HSPC emergence but not in earlier vascular patterning or specification of the DA.

vegfc loss-of-function embryos show decreased *cd41:gfp*+ HSPCs in the CHT

After observing a significant decrease in HSPCs in the DA, we wanted to determine if the effects of *vegfc* loss-of-function are maintained throughout development. After emergence from the DA, HSPCs migrate through circulation to seed the CHT where they expand in number (Ciau-Uitz et al., 2014, Murayama et al., 2006). Using the HSPC transgenic reporter line *cd41:gfp* we observed significantly fewer *cd41:gfp*$^{+}$ cells in the CHT of *vegfc* loss-of-function embryos (Fig. 2A,B and S7A,B). The decrease in *cd41:gfp*$^{+}$ cell lodgment in the CHT was not due to defective EC pocket formation (Tamplin et al., 2015), as these niche structures were still present in *vegfc* loss-of-function embryos (Fig. S7C,D). Decreased HSPCs were further confirmed using our scRNA-seq datasets from control and *vegfc* loss-of-function *flk:mCherry;cd41:gfp* embryos (Fig. S2 and S3). The percentage of cells in the HSPC cluster was lower in *vegfc* morphants (5%) compared to controls (12%) (Fig. S2C).

We wanted to determine if this decrease in HSPC emergence and colonization of the CHT indicated a sustained reduction in definitive hematopoiesis. We assessed *rag1* expression in the 5 dpf thymus, as thymic seeding is dependent on the emergence of definitive HSPCs from the DA (Jin et al., 2007, Murayama et al., 2006). *vegfc* crispant and morphant embryos had significantly lower *rag1* expression than control embryos (Fig. 2C,D and S7E,F). To further confirm the specificity of our genetic tools, we attempted to rescue definitive hematopoiesis in *vegfc* morphants using a MO-resistant *vegfc* mRNA (Fig. S8A). Co-injection of *vegfc* MO with either 200 or 400 pg of rescue mRNA dose-dependently restored *rag1* expression in the thymus at 5 dpf (Fig. S8B,C). To confirm the specificity of *vegfc* crispants, we co-injected the same *vegfc* MO-resistant mRNA and measured *rag1* expression at 5 dpf. Injection of *vegfc* mRNA was able to restore *vegfc* crispant *rag1* expression to control levels (Fig. S8D,E). Finally, we wanted to determine if over-expression of *vegfc* would increase HSPC numbers. We injected the same *vegfc* MO-resistant mRNA and quantified *cd41:gfp* cells at 72 hpf, but observed no change (Fig. S8H,I). As expected, some of the *vegfc* mRNA injected embryos exhibited altered vascular morphology (data not shown), likely due to hyper-proliferation of venous derived ECs (Grimm et al., 2019). Together, these data show *vegfc* morphant and crispant phenotypes faithfully recapitulate genetic mutant alleles. Furthermore, loss-of-function embryos show

impaired definitive hematopoiesis beginning with reduced HSPC emergence in the DA and persisting through to progenitor seeding of the thymus at 5 dpf.

To further interrogate definitive hematopoiesis in the CHT of *vegfc* loss-of-function embryos, we examined expression of the *cmyb* marker by WISH. Interestingly, in contrast to the decrease of *cd41:gfp*+ cells we observed in the CHT of *vegfc* crispant (Fig. 2A,B) and morphant (Fig. S7A,B) embryos, there were significantly more *cmyb*+ cells in *vegfc* crispants (Fig. 2E,F), *vegfc*^{um18} null (Fig. 2G,H), and *vegfc* morphant embryos (Fig. S7G,H) compared to controls. We performed a rescue experiment in *vegfc* morphants and saw that co-injection of *vegfc* MO and MO-resistant *vegfc* mRNA, but not control mRNA, could rescue *cmyb* expression (Fig. S8F,G). We wanted to resolve opposing results between *cd41:gfp*+ and *cmyb*+ WISH as HSPC markers in the CHT of *vegfc* loss-of-function embryos. Studies in chicken embryos showed that *cmyb* marks myeloid cells in addition to HSPCs (Duprey and Boettiger, 1985). Therefore, we wanted to test the hypothesis that increased *cmyb* expression resulted in part from an increase in myeloid progenitor cells. We used *cmyb:gfp;lyz:DsRed2* embryos to visualize putative *cmyb:gfp*+ HSPCs together with *lyz:DsRed2*+ myeloid cells in the same embryo (Fig. S9A). We found that 55.87% ± 2.16 of cells are *cmyb:gfp*+, 44.12% ± 2.16 are *lyz:DsRed2*+, and 34.70% ± 1.79 are double positive (Fig. S9B). We identified HSPCs by their round shape and expression of *cmyb:gfp* alone. We considered myeloid cells as *lyz:DsRed2*+ that were positive or negative for *cmyb:gfp.* Next, we used *cd41:gfp;lyz:DsRed2* embryos to determine if the *cd41:gfp* transgenic line also marked myeloid cells in addition to HSPCs (Fig. S9C). We found that 48.13% ± 1.96 of cells are *cd41:gfp*$^{+}$, 51.86% ± 1.96 are *lyz:DsRed2*$^{+}$, and we found none that were double positive (Fig. S9D). These results suggest that *cd41:gfp* is a more specific reporter for HSPCs than *cmyb:gfp*. Furthermore, while *vegfc* loss-of-function embryos have decreased *cd41:gfp*+ HSPC numbers, the increase in *cmyb*+ WISH expression suggests abundance of myeloid progenitors.

vegfc loss-of-function embryos have an increase in myeloid progenitors

We wanted to further characterize the possible increase in myeloid progenitors upon *vegfc* loss-of-function. First, we examined the myeloid marker *mpx* by WISH and found there was a significant increase in *vegfc* loss-of-function embryos in the CHT at 56 hpf, compared to Cas9 controls (Fig. 3A,B). Genetic mutant *vegfc*^{um18} and *vegfc* morphant embryos also showed an increase in *mpx*$^{+}$ cells in the CHT at 56 hpf (Fig. 3C,D and S10A,B). This was consistent with our finding that a proportion of the increased *cmyb:gfp*+ cells in *vegfc* loss-of-function embryos are likely myeloid progenitors (Fig 2E-H and S7G,H), as suggested by the colocalization of *cmyb:gfp* with myeloid marker *lyz:DsRed2* (S9A,B). To further confirm increased *mpx* expression in the CHT, we used the transgenic line *lyz:DsRed2* to visualize myeloid cells at 72 hpf and saw an increased number of *lyz:DsRed2*+ cells in the CHT of *vegfc* loss-of-function embryos (Fig. 3E,F). This was also confirmed using *mpx:gfp*+ cells in *vegfc* morphants (Fig. S10C,D). Increased myeloid cells were further confirmed using our scRNA-seq dataset. The *mpx*+ cluster of myeloid cells (Fig. S2B cluster #5 and S3A), showed an increase in the total proportion of cells in *vegfc* morphants (7%) compared to controls (3%) (Fig. S2C). We were also interested in how overexpression of *vegfc* would impact myeloid numbers in the CHT. To do

this, we injected embryos with the same *vegfc* rescue mRNA described above and quantified the number of *mpx*+ cells in the CHT at 72 hpf. Overexpression of *vegfc* resulted in decreased *mpx*+ cells compared to controls (Fig. 3G,H). The observed increase or decrease in myeloid progenitors with vegfc loss-of-function or overexpression, respectively, suggests that *vegfc* could play a role in regulating hematopoietic fate decisions.

We next wanted to determine if *vegfc* loss-of-function results in an overall myeloid bias, or if it is specific to neutrophils or macrophages. In order to determine if neutrophil numbers were impacted, we used Sudan black B stain, a lipophilic stain that binds to granulocytes of neutrophils (Swirsky and Bain, 2006). Loss of *vegfc* resulted in significantly more stained cells in the CHT than uninjected controls (Fig. S10E,F). We used the transgenic line *mpeg:gfp* to investigate macrophage numbers in *vegfc* loss-of-function embryos and found a significant increase in the CHT (Fig. S10G,H). We saw increased numbers of both CHT neutrophils and macrophages suggesting that *vegfc* loss-of-function results in an overall increase in myeloid cells.

Neutrophils in *vegfc* loss-of-function embryos have an altered injury response

After observing that *vegfc* loss-of-function embryos have more CHT myeloid cells than control embryos, we wanted to investigate if they are still functional and able to respond to injury. Caudal fin transection is an *in vivo* injury model of inflammation and wound repair that produces a robust and well-characterized neutrophil response (Isles et al., 2019, Miskolci et al., 2019, Ellett et al., 2015). We transected a portion of the caudal fin at 72 hpf and fixed embryos at 2, 6, and 24 hours post injury (hpi) (Fig. 4A). Control embryos showed a typical pattern of response, with the number of neutrophils at the site of injury peaking at 6 hpi (Fig. 4B,D). Embryos with *vegfc* loss-of-function showed an altered timing with their response peaking at 2 hpi and diminishing over 24 hours (Fig. 4C,D). Both treatment groups resolved injury at 24 hpi with no statistical difference in the number of neutrophils in the wound area (Fig. 4D). The higher number of neutrophils at the injury site of *vegfc* loss-of-function embryos at 2 hpi may be explained by the higher number of available neutrophils in the CHT (Fig. 4E,F), or more rapid migration to the site of injury. Our results demonstrate that the neutrophils in *vegfc* loss-of-function embryos are still able to respond to injury and migrate to the wound site.

vegfc loss-of-function embryos show altered HSPC behavior in the DA

We wanted to determine the origin of increased myeloid cells in *vegfc* loss-of-function embryos. We considered that HE cells failing to undergo EHT in *vegfc* loss-of-function embryos during the peak of emergence (Fig. 1; 48-52 hpf), may persist in the DA until later stages. To resolve this, we performed time-lapse imaging of the DA during a later time window from 56–72 hpf. During later stage EHT in control embryos we still observed cells budding from the DA, however the frequency was reduced from ~3 per hour between 48-52 hpf, to less than one per hour between 56–72 hpf (compare Fig.1C, 5C, and S11C). Although there was no significant difference in the number of budding cells between control and *vegfc* loss-of-function embryos from 56–72 hpf,

we did observe a significant increase in the number of cells that exhibited crawling behavior in *vegfc* loss-of-function embryos (Fig. 5A-C and S11A-C; Movies 3 and 4). Comparison of late stage HE shows very different morphology between control and *vegfc* loss-of-function embryos, with the latter showing increased *cd41:gfp*+ cell movement and altered cell morphology. Time-lapse imaging showed that *vegfc* loss-of-function resulted in cells of the ventral wall of the DA extending filopodia and crawling around the cardinal vein, instead of rounding up and budding off into circulation as in controls (Fig. 5A,B and S11A,B; Movies 3 and 4). Crawling cells appear to have decreased *cd41:gfp* intensity compared to budding HSPCs that we hypothesize have down-regulated the HSPC-specific *cd41* promoter as they differentiate towards a myeloid fate. *vegfc* loss-of-function embryos showed a significant increase in *flk:mCherry+;cd41:gfp*+ HE cells that were crawling out of the DA and around the CV (Fig. 5C and S11C). The number of *flk:mCherry*$^{+}$*;cd41:gfp*$^{+}$ budding cells were not significantly different (Fig. 5C and S11C).

We wanted to find if the increase in crawling cells in the DA was consistent with an increase in myeloid progenitors. We performed time-lapse imaging of *lyz:DsRed2;flk:gfp* embryos from 54-72 hpf and quantified the number of *lyz:DsRed2*+ cells residing in the DA. In *vegfc* loss-of-function embryos we saw significantly more *lyz:DsRed2*+ crawling cells in the ventral wall of the DA, as compared to Cas9 controls (Fig 5D,E; Movies 5,6). To further confirm the identity of *lyz:DsRed2*+ cells in the DA, we performed a co-localization experiment with *cd41:gfp*. Cells that resided within the DA were double positive for *lyz:DsRed2;cd41:gfp* and there was a higher number of these cells in *vegfc* loss-of-function embryos compared to controls (Fig 5F,G). To further validate the presence of these putative myeloid progenitors in the HE we examined expression of *mpx* at 56 hpf. The majority of *vegfc* loss-of-function embryos expressed *mpx* in the DA (>60%), compared to very few control embryos (<10%; Fig. S11D,E). These results suggest that the abundance of myeloid cells in *vegfc* loss-of-function embryos originate from an altered fate in the DA.

Inhibition of vegf family receptors phenocopies *vegfc* loss-of-function

We wanted to gain insight into the receptors that mediate vegfc signal in the HE. Recent zebrafish studies showed that flt4/vegfr3 and kdr, but not kdrl, are vegfc targets (Vogrin et al., 2019). We examined *cmyb* expression in the CHT of *flt4/vegfr3* mutants at 72 hpf but did not see any difference in expression (Fig. S12). These data, together with published expression data showing that *flt4/vegfr3* is expressed in the cardinal vein and not the DA (Gore et al., 2011), suggest that *flt4/vegfr3* is not the key receptor for vegfc signaling in the DA. Next, we treated embryos with the pan-vegf receptor inhibitor SU5416 (Sukbuntherng et al., 2001, Serbedzija et al., 1999). There is an early requirement for vegf receptors in patterning the vasculature and DA, and therefore the HE itself, so we started SU5416 treatments later at 32 hpf (Fig. 6A). Next, we performed time-lapse live imaging from 48 to 52 hpf of multiple *flk:mCherry/cd41:gfp* embryos in parallel that were vehicle or SU5416-treated. The number of HSPCs that emerged from the DA was significantly reduced in SU5416-treated embryos (Fig. 6B,C). We did not see any vascular defects or disrupted blood flow in SU5416-treated embryos (Fig. 6B and data not shown). Consistent with reduced HSPC production from the DA, we observed fewer *cd41:gfp*+ cells in the CHT later at 72 hpf (Fig. 6D,E). Similar to *vegfc* loss-of-

function embryos, SU5416-treated embryos also had increased expression of *cmyb* (compare Fig. 6F,G and 2E-H) and *mpx* (compare Fig. 6H,I and 3A-D) by WISH at 72 hpf. The comparable decrease in *cd41:gfp*+ HSPCs and increase in *mpx*+ myeloid progenitors, in both *vegfc* loss-of-function and SU5416-treated embryos, suggests that the vegfc-vegf receptor signaling axis plays a role in HE fate decisions and the emergence of HSPCs.

Discussion

Many studies have investigated the mechanics of HSPC emergence from the HE, but it is unclear what factors maintain HSPC fate and prevent premature differentiation. Our goal was to investigate the potential role of VEGFC in maintaining HSPC fate, based on its expression within the DA and undifferentiated HSPCs. Currently, the majority of VEGFC studies have detailed its role in lymphangiogenesis (Karkkainen et al., 2004, Küchler et al., 2006, Jeltsch et al., 1997). A few studies in mice have examined the role of VEGFC in hematopoiesis (Hamada et al., 2000, Fang et al., 2016, Fang et al., 2020). In our study, we provide evidence in zebrafish that vegfc plays a role in regulating HSPC fate decisions during emergence from the DA.

In zebrafish it is thought that HE specification begins with pre-HE cells that contact the somites, before the DA is formed (Clements et al., 2011, Kobayashi et al., 2014). This physical contact is crucial for notch signaling and subsequent specification of HE cells. Loss-of-function of somite-mesoderm cell adhesion factors decreases HSPC numbers (Kobayashi et al., 2014). In chick and mouse, once the DA is formed, the action of mesenchymal-derived VEGF on VEGFR2 acts as a pro-hematopoietic ventralizing factor (Pardanaud and Dieterlen-Lièvre, 1999, Peeters et al., 2009). In studies by Hamada et al. that used para-aortic splanchnopleural mesoderm (P-Sp) explants, addition of exogenous VEGFC to WT explants suppressed hematopoiesis (Hamada et al., 2000). In the mouse embryo there is likely complex synergism between VEGF and VEGFC as they both bind VEGFR2 and FLT4/VEGFR3 to regulate early vascular and hematopoietic development (Hamada et al., 2000). In zebrafish, vegfc is thought to bind flt4/vegfr3 and kdr, but not kdrl (Vogrin et al., 2019). Our results would suggest a role for vegfc after specification of the HE to maintain HSPC fate throughout the full duration of EHT.

In our study, we have shown that embryos lacking *vegfc* have decreased emergence of HSPCs from the HE. The process of HSPC specification appears to be intact in *vegfc* loss-of-function embryos, as *cd41:gfp*$^{+}$ cells are still present within the HE and a small number of HSPCs are still produced. However, many of these HE cells do not complete EHT, as the exiting cell appears stuck in the ventral wall of the DA. Normally during EHT the neighboring rostral and caudal ECs join to maintain continuity in the ventral wall of the DA and aid in HSPC release (Kissa and Herbomel, 2010). This joining of ECs does not appear to occur in *vegfc* loss-of-function embryos, perhaps because they lack the mechanical organization of actin that is required for cell emergence (Lancino et al., 2018). The reduced number of definitive HSPCs persists until larval stages, suggesting that emergent HSPCs stuck in the DA do not recover.

Although *vegfc* loss-of-function embryos have fewer HSPCs, they have a greater number of myeloid progenitors that emerge later from the DA and populate the CHT. We used a caudal fin transection injury model to determine if *vegfc* loss-of-function embryos produced functional neutrophils (Isles et al., 2019, Ellett et al., 2015). After injury, neutrophil wound response typically peaks at around 6 hpi (Miskolci et al., 2019, Li et al., 2012). In control embryos we saw the expected peak at 6 hpi, however injured *vegfc* loss-of-function embryos exhibited a neutrophil wound response that peaked earlier at 2 hpi. The specific reason for this altered wound response timing is still not clear, however the neutrophils were still functional in their migration to the site of injury. We speculate that their altered response pattern is due to either faster migration or an increased number of neutrophils in the CHT that are ready to respond to injury.

vegfc loss-of-function embryos show an overproduction of myeloid progenitors that appears to originate from HE. There are a small number of myeloid progenitor cells that normally emerge from the DA (Jin et al., 2009), and these crawling cells are visible in previously published time-lapse live imaging data sets (Lancino et al., 2018, Bertrand et al., 2010). In *vegfc* loss-of-function embryos there are significantly more of these crawling myeloid progenitors produced by the DA. Alternate fates produced from HE of the mouse have been identified, as there are HE-derived HSC precursors that display a B-1 lymphoid bias and go on to differentiate to multi-potent progenitors in the FL (Kobayashi et al., 2019). The increase of both *lyz:DsRed2*+ cells and *mpx* expression in the DA of *vegfc* loss-of-function embryos suggests that *vegfc* is involved in regulating HE fate decisions in late-stage DA.

In summary, we propose that VEGFC plays a role in maintaining HSPC fate during emergence from the DA. Based on scRNA-seq of mouse cells from endothelium to HSPCs, *Vegfc* is most highly expressed in pre-HE cells (Zhu et al., 2020). In zebrafish, HSPC emergence from the DA peaks at 48 hpf and then decreases by 56 hpf and there are few myeloid-like crawling cells that emerge. This output is reflected in the CHT with similar numbers of HSPCs and myeloid cells (Fig. 7A). However, with *vegfc* loss-of-function, there are fewer HSPCs produced during the peak of emergence, and by 56 hpf there are many myeloid-like crawling cells that emerge from the DA. In these embryos, the CHT has an overwhelming dominance of myeloid cells, with few HSPCs (Fig. 7B). Our model supports a novel role for VEGFC in maintaining HSPC fate in the HE. A better understanding of the factors that regulate HE development are critical for optimizing *in vitro* differentiation of pluripotent stem cells into HSPCs (Slukvin, 2013, Ditadi et al., 2017). The ability to promote HSPC versus myeloid fate *in vitro* using VEGFC may have the potential to improve pluripotent stem cell differentiation protocols.

Materials and Methods

Fish care

Zebrafish were maintained at the University of Illinois at Chicago and University of Wisconsin-Madison in accordance with their respective Institutional Animal Care and Use Committee guidelines. Zebrafish were mated, staged and raised as previously described (Westerfield, 2000). Adult wild-type (wt) (AB strain), *vegfc*^{um18} mutants (Villefranc et al., 2013), and the following transgenic lines were used in this study: *Tg(cd41:gfp)* aka *la2Tg* or *Tg(-6.0itga2b:eGFP)* (Lin et al., 2005); *Tg(flk:mCherry)* aka *s896Tg* or *Tg(flk1:ras-cherry)* (Chi et al., 2008); *Tg(mpx:gfp)* aka *uwm1Tg* or *Tg(mpx:GFP)uwm1* (Mathias et al., 2006); *Tg(lyz:DsRed2)* aka *nz50Tg* or *Tg(lysC:DsRed2)nz50* (Hall et al., 2007); *Tg(cmyb:gfp)* aka *zf169Tg* or *Tg(cmyb:GFP)unspecified* (North et al., 2007); *Tg(mpeg:gfp)* aka *gl22Tg* or *Tg(mpeg1:EGFP)gl22* (Ellett et al., 2011); *Tg(tp1:dGFP) aka Tg(EPV.Tp1-Mmu.Hbb:Venus-Mmu.Odc1)* (Ninov et al., 2012). *vegfc*^{um18} mutant carriers were genotyped by PCR amplification and Sanger sequencing.

Microinjections of zebrafish embryos

MO targeting the *vegfc* start codon ATG MO, 5'-GAAAATCCAAATAAGTGCATTTTAG-3' was purchased from GeneTools (Ober et al., 2004). Standard control MO targeting a human beta-globin intron mutation, 5'-CCTCTTACCTCAGTTACAATTTATA-3' was purchased from GeneTools. MO stock solutions were prepared at 1 mM and heated for 10' at 65°C before preparing injection mix to ensure a uniform solution. Embryos were injected with 4 ng of MO at the 1-cell stage and compared to uninjected sibling controls. Rescue *vegfc* mRNA was designed to be MO resistant so that the third base pair of each codon was altered to inhibit MO binding but preserve amino acid sequence. The gene sequence was ordered from Genscript and linearized using the *NotI* restriction enzyme (NEB). mRNA was transcribed using an mMessage mMachine SP6 kit (Invitrogen). *vegfc* MO (4ng/nl) and rescue mRNA (200 pg/nl or 400 pg/nl) was injected sequentially at the one cell stage. Tol2 mRNA at the same concentration as rescue mRNA was used as a negative control.

Whole mount in situ hybridization (WISH)

Embryos were stage matched and fixed overnight at 4°C in 4% PFA. Whole mount *in situ* hybridization was performed as previously described (Thisse and Thisse, 2008) with the following exceptions: before permeabilization with proteinase K, embryos were bleached to remove pigmentation and 0.2% glutaraldehyde was added to 4% formaldehyde at the post-fixation step. Antisense RNA probes *cmyb* (Liao et al., 1998), *mpx* (Lieschke et al., 2001), and *rag1* (Willett et al., 1997) were used as previously described. WISH images were quantified using the Cell Counter or Measure features of Fiji/ImageJ. DIC images were obtained as described below.

Cell preparation for single-cell RNA sequencing

Whole 52 hpf *flk:mCherry/cd41:gfp*+ embryos were dissociated into a single cell suspension for fluorescence activated cell sorting (FACS) as previously described (Bresciani et al., 2018) with the following exceptions: additional filter step added prior to centrifugation in step 2.3 and final resuspension of single cells was done in PBS + 2% FBS. The control sample comprised of 4,000 each of uninjected *flk:mCherry*+ and *cd41:gfp*+ cells and the *vegfc* MO sample comprised of 4,000 each of *vegfc* MO *flk:mCherry*+ and *cd41:gfp*+ cells. Then single cell suspensions were loaded on a Chromium Single Cell Controller (10x Genomics) to generate single-cell gel beads in emulsion (GEMs) by using Single Cell 3' Library and Gel Bead Kit V3.1 (10x Genomics, 1000121). Cell lysis and RNAs barcoding were accomplished through reverse transcription in individual GEMs. Barcoded cDNAs were pooled and cleaned up using SPRIselect beads (Beckman Coulter, B23317). Single-cell RNA-seq libraries were prepared using Single Cell 3' v3.1 Reagents Module 2 (10x Genomics, 1000121) following the manufacturer's instructions. Sequencing was performed on an Illumina NovaSeq 6000 with paired end 150 bp (PE150).

Single Cell RNA-seq Analysis

CellRanger (5.0.0) was used to generate gene expression containing unique molecular identifies (UMIs) matrix using the default parameters. We used a custom zebrafish reference genome (custom_GRCz11_reporters) that included the transgenes EGFP and mCherry. Samples were then further filtered and clustered in Seurat (Stuart et al., 2019). Cells with a feature count between 200 and 3,500 and a mitochondrial gene percentage less than 18% were used in analysis, resulting in 5,655 high quality single cells. Then, we selected 2,000 most variable genes and fed into Seurat for dimension reduction by PCA. We ran "RunPCA" to identify significant principal components (PC). The top 10 PCs were selected for t-SNE clustering. The "FindClusters" function was run to find the cell clusters at 0.5 resolution. Cluster identity was assigned manually using known marker genes.

sgRNA design and synthesis

CCTop, E-Crisp and CHOPCHOP were used to identify single guide RNA (sgRNA) sequences with high on-target activity. Sequence specificity was then confirmed using IDTs software to predict off-target activity and sgRNAs with highest on-target and lowest off-target activities. We chose the following sequence in exon 2 of *vegfc*: GGATAGTTTACCCTACCTAC Pam: CGG. sgRNA was purchased from IDT for the generation of F0 crispants. Primers: Forward: 5'-ACACTCTTTCCCTACACGACGCTCTTCCGATCTagcatcaaaatctcttggctgt-3'. Reverse: 5'-GTGACTGGAGTTCAGACGTGTGCTCTTCCGATCTgtcaatgttagtatggggcaca-3'. Lowercase letters indicate primers sequences that are specific to the *vegfc* locus and span a 374 bp region covering the sgRNA target region. Underlined sequences are Illumina 5'-3' Multiplexing Read 1 and 2 adapter sequences, respectively. RNP was assembled and injected as previously described (Burger et al., 2016). We assessed mutagenesis of our sgRNA sequence by extracting genomic DNA from a minimum of 15 embryos and performing Illumina MiSeq

sequencing. We then used CRISPResso2 to align and compare the reads (Clement et al., 2019).

Sudan Black staining

Embryos were fixed overnight at 4C in 4% PFA. Sudan black stain was performed as previously described (Rosowski et al., 2018). DIC images were obtained as described below.

Imaging

Transgenic zebrafish lines were crossed, and staged embryos were selected by fluorescence microscopy. Embryos were anesthetized in 0.04% tricaine and mounted for live imaging in glass bottomed dishes or multi-well plates in 1% low-melt agarose and covered with E3 media and tricaine as previously described (Bertrand et al., 2010). The zebrafish embryos were maintained at 28.5°C in an incubated stage. Live time-lapse microscopy was performed using a Zeiss Spinning Disk Confocal using a 20X Plan-Apochromat objective or a Nikon Yokogawa CSU-W1 Spinning Disk Confocal using a 20X objective. Timepoints were recorded every 3-4 minutes for the stated time period. WISH and Sudan Black stained embryos were mounted in 70% glycerol and imaged on a Nikon SMZ18 stereoscope at 4x for whole embryo images and 8x for regional imaging. All confocal images shown are max projection in Z.

Image Analysis

Images were processed and analyzed using Zen (Zeiss), Elements (Nikon), Imaris (Bitplane) and Fiji/ImageJ. Confocal z-stack images are presented as maximum projections. Cell tracking and counting was performed using Imaris spot detection feature. For cell behavior quantification, DA derived *flk:mCherry/cd41:gfp* double positive cells were quantified based on behavior and classified as either budding or crawling. To be classified as crawling, cells must extend filopodia and move contrary to blood flow in the caudal vein; to be classified as budding, cells must emerge and immediately enter circulation.

Drug Treatments

SU5416 (Cayman Chemical, 13342) were dissolved in DMSO and stored at −20°C. Embryos were treated from 32 hpf until 72 hpf with 0.75 uM SU5416. 0.1% DMSO alone was used as a control. All treatments were diluted in E3 medium. ***Drug Treatments***

SU5416 (Cayman Chemical, 13342), LY294 (Sigma-Aldrich, L9908) , SL327 (Cayman Chemical, 15598) and DAPT (Cayman Chemical, 13197) were dissolved in DMSO and stored at −20°C. *flk:mCherry;cd41:gfp* embryos were treated from 32 hpf until 72 hpf with either 0.75 uM SU5416, 5 uM LY294, 10 uM SL327 or 10 uM DAPT. 0.1% DMSO alone was used as a control. All treatments were diluted in E3 medium.

Statistical Analysis

Statistical analysis was done using Graph Pad Prism V7.0 or R Studio 1.2. Data are presented as mean±SEM. Analysis of two experimental groups were done using a students t-test. Analysis of more than two experimental groups were done using one-way ANOVA, with multiple comparisons. Low / high expression analysis of WISH experiments was done in R Studio using a chi-squared goodness of fit test. p-values are indicated in the figures.

Acknowledgements

We would like to thank Dr. Nathan Lawson for sharing the *vegfc*^{um18} zebrafish line and Dr. Teresa Bowman for sharing the *mpx:gfp*, *cmyb:gfp*, and *lyz:DsRed2* transgenic zebrafish lines. Microscopy was performed at The University of Illinois at Chicago RRC Fluorescence Imaging Core and The University of Wisconsin-Madison Optical Imaging Core. Sequencing of genetic mutants was performed at The University of Illinois at Chicago RRC Genome Research Core. We acknowledge the University of Wisconsin-Madison Biotechnology Center Gene Expression Center, DNA Sequencing Facility, and Bioinformatics Resource Center for providing scRNA-seq library preparation, next generation sequencing services, and data analysis. We acknowledge the University of Wisconsin Carbone Cancer Center Support Grant P30 CA014520 for the Flow Cytometry Laboratory. R.K.S. Contributions: Conceptualization, Methodology, Validation, Formal analysis, Investigation, Data curation, Writing - original draft, Visualization. O.J.T. Contributions: Conceptualization, Methodology, Resources, Writing - review editing, Supervision, Project administration, Funding acquisition.

Competing interests

The authors have no competing interests to declare.

Funding

Research reported in this publication was supported by the National Institutes of Health: National Heart, Lung, and Blood Institute [R01HL142998 to O.J.T, T32HL027829 to R.K.S.], and the National Institute of Diabetes and Digestive and Kidney Diseases [K01DK103908 to O.J.T]. It was also supported by an American Society of Hematology (ASH) Junior Faculty Scholar Award [O.J.T.]. Additional funding was provided by the University of Illinois at Chicago and the University of Wisconsin-Madison.

Data availability

Raw and processed scRNA-seq data has been deposited in the NCBI GEO database (GSE186565).

References

BAHARY, N., GOISHI, K., STUCKENHOLZ, C., WEBER, G., LEBLANC, J., SCHAFER, C. A., BERMAN, S. S., KLAGSBRUN, M. & ZON, L. I. 2007. Duplicate VegfA genes and orthologues of the KDR receptor tyrosine kinase family mediate vascular development in the zebrafish. *Blood,* 110**,** 3627-36.

BATSIVARI, A., RYBTSOV, S., SOUILHOL, C., BINAGUI-CASAS, A., HILLS, D., ZHAO, S., TRAVERS, P. & MEDVINSKY, A. 2017. Understanding Hematopoietic Stem Cell Development through Functional Correlation of Their Proliferative Status with the Intra-aortic Cluster Architecture. *Stem Cell Reports,* 8**,** 1549-1562.

BERTRAND, J. Y., CHI, N. C., SANTOSO, B., TENG, S., STAINIER, D. Y. R. & TRAVER, D. 2010. Haematopoietic stem cells derive directly from aortic endothelium during development. *Nature,* 464**,** 108-111.

BOISSET, J.-C., VAN CAPPELLEN, W., ANDRIEU-SOLER, C., GALJART, N., DZIERZAK, E. & ROBIN, C. 2010. In vivo imaging of haematopoietic cells emerging from the mouse aortic endothelium. *Nature,* 464**,** 116-120.

BRESCIANI, E., BROADBRIDGE, E. & LIU, P. P. 2018. An efficient dissociation protocol for generation of single cell suspension from zebrafish embryos and larvae. *MethodsX,* 5**,** 1287-1290.

BURGER, A., LINDSAY, H., FELKER, A., HESS, C., ANDERS, C., CHIAVACCI, E., ZAUGG, J., WEBER, L. M., CATENA, R., JINEK, M., ROBINSON, M. D. & MOSIMANN, C. 2016. Maximizing mutagenesis with solubilized CRISPR-Cas9 ribonucleoprotein complexes. *Development (Cambridge, England),* 143**,** 2025-2037.

CHI, N. C., SHAW, R. M., DE VAL, S., KANG, G., JAN, L. Y., BLACK, B. L. & STAINIER, D. Y. 2008. Foxn4 directly regulates tbx2b expression and atrioventricular canal formation. *Genes Dev,* 22**,** 734-9.

CIAU-UITZ, A., MONTEIRO, R., KIRMIZITAS, A. & PATIENT, R. 2014. Developmental hematopoiesis: Ontogeny, genetic programming and conservation. *Experimental Hematology,* 42**,** 669-683.

CLEMENT, K., REES, H., CANVER, M. C., GEHRKE, J. M., FAROUNI, R., HSU, J. Y., COLE, M. A., LIU, D. R., JOUNG, J. K., BAUER, D. E. & PINELLO, L. 2019. CRISPResso2 provides accurate and rapid genome editing sequence analysis. *Nat Biotechnol,* 37**,** 224-226.

CLEMENTS, W. K., KIM, A. D., ONG, K. G., MOORE, J. C., LAWSON, N. D. & TRAVER, D. 2011. A somitic Wnt16/Notch pathway specifies haematopoietic stem cells. *Nature,* 474**,** 220-224.

COVASSIN, L. D., VILLEFRANC, J. A., KACERGIS, M. C., WEINSTEIN, B. M. & LAWSON, N. D. 2006. Distinct genetic interactions between multiple Vegf receptors are required for development of different blood vessel types in zebrafish. *Proceedings of the National Academy of Sciences of the United States of America,* 103**,** 6554-6559.

DITADI, A., STURGEON, C. M. & KELLER, G. 2017. A view of human haematopoietic development from the Petri dish. *Nature Reviews Molecular Cell Biology,* 18**,** 56-67.

DUPREY, S. P. & BOETTIGER, D. 1985. Developmental regulation of c-myb in normal myeloid progenitor cells. *Proc Natl Acad Sci U S A,* 82**,** 6937-41.

ELLETT, F., ELKS, P. M., ROBERTSON, A., OGRYZKO, N. V. & RENSHAW, S. 2015. Defining the phenotype of neutrophils following reverse migration in zebrafish. *Journal of Leukocyte Biology,* 98**,** 975 - 981.

ELLETT, F., PASE, L., HAYMAN, J. W., ANDRIANOPOULOS, A. & LIESCHKE, G. J. 2011. mpeg1 promoter transgenes direct macrophage-lineage expression in zebrafish. *Blood,* 117**,** e49-e56.

EMA, H. & NAKAUCHI, H. 2000. Expansion of hematopoietic stem cells in the developing liver of a mouse embryo. *Blood,* 95**,** 2284-2288.

FANG, S., CHEN, S., NURMI, H., LEPPÄNEN, V. M., JELTSCH, M., SCADDEN, D., SILBERSTEIN, L., MIKKOLA, H. & ALITALO, K. 2020. VEGF-C protects the integrity of the bone marrow perivascular niche in mice. *Blood,* 136**,** 1871-1883.

FANG, S., NURMI, H., HEINOLAINEN, K., CHEN, S., SALMINEN, E., SAHARINEN, P., MIKKOLA, H. K. A. & ALITALO, K. 2016. Critical requirement of VEGF-C in transition to fetal erythropoiesis. *Blood*.

GARCIA-PORRERO, J. A., GODIN, I. E. & DIETERLEN-LIÈVRE, F. 1995. Potential intraembryonic hemogenic sites at pre-liver stages in the mouse. *Anat Embryol (Berl),* 192**,** 425-35.

GAZIT, R., GARRISON, B. S., RAO, T. N., SHAY, T., COSTELLO, J., ERICSON, J., KIM, F., COLLINS, J. J., REGEV, A., WAGERS, A. J., ROSSI, D. J. & IMMUNOLOGICAL GENOME PROJECT, C. 2013. Transcriptome analysis identifies regulators of hematopoietic stem and progenitor cells. *Stem Cell Reports,* 1**,** 266-80.

GORE, A. V., SWIFT, M. R., CHA, Y. R., LO, B., MCKINNEY, M. C., LI, W., CASTRANOVA, D., DAVIS, A., MUKOUYAMA, Y. S. & WEINSTEIN, B. M. 2011. Rspo1/Wnt signaling promotes angiogenesis via Vegfc/Vegfr3. *Development,* 138**,** 4875-86.

GRIMM, L., NAKAJIMA, H., CHAUDHURY, S., BOWER, N. I., OKUDA, K. S., COX, A. G., HARVEY, N. L., KOLTOWSKA, K., MOCHIZUKI, N. & HOGAN, B. M. 2019. Yap1 promotes sprouting and proliferation of lymphatic progenitors downstream of Vegfc in the zebrafish trunk. *Elife,* 8.

HALL, C., FLORES, M. V., STORM, T., CROSIER, K. & CROSIER, P. 2007. The zebrafish lysozyme C promoter drives myeloid-specific expression in transgenic fish. *BMC Developmental Biology,* 7**,** 42.

HAMADA, K., OIKE, Y., TAKAKURA, N., ITO, Y., JUSSILA, L., DUMONT, D. J., ALITALO, K. & SUDA, T. 2000. VEGF-C signaling pathways through VEGFR-2 and VEGFR-3 in vasculoangiogenesis and hematopoiesis. *Blood,* 96**,** 3793-3800.

HOGAN, B. M., BOS, F. L., BUSSMANN, J., WITTE, M., CHI, N. C., DUCKERS, H. J. & SCHULTE-MERKER, S. 2009. Ccbe1 is required for embryonic lymphangiogenesis and venous sprouting. *Nature genetics,* 41**,** 396-398.

ISLES, H. M., HERMAN, K. D., ROBERTSON, A. L., LOYNES, C. A., PRINCE, L. R., ELKS, P. M. & RENSHAW, S. A. 2019. The CXCL12/CXCR4 Signaling Axis Retains Neutrophils at Inflammatory Sites in Zebrafish. *Frontiers in Immunology,* 10.

JELTSCH, M., KAIPAINEN, A., JOUKOV, V., MENG, X., LAKSO, M., RAUVALA, H., SWARTZ, M., FUKUMURA, D., JAIN, R. K. & ALITALO, K. 1997. Hyperplasia of lymphatic vessels in VEGF-C transgenic mice. *Science,* 276**,** 1423-5.

JIN, H., SOOD, R., XU, J., ZHEN, F., ENGLISH, M. A., LIU, P. P. & WEN, Z. 2009. Definitive hematopoietic stem/progenitor cells manifest distinct differentiation output in the zebrafish VDA and PBI. *Development (Cambridge, England),* 136**,** 647-654.

JIN, H., XU, J. & WEN, Z. 2007. Migratory path of definitive hematopoietic stem/progenitor cells during zebrafish development. *Blood,* 109**,** 5208-5214.

JOUKOV, V., PAJUSOLA, K., KAIPAINEN, A., CHILOV, D., LAHTINEN, I., KUKK, E., SAKSELA, O., KALKKINEN, N. & ALITALO, K. 1996. A novel vascular endothelial growth factor, VEGF-C, is a ligand for the Flt4 (VEGFR-3) and KDR (VEGFR-2) receptor tyrosine kinases. *EMBO J,* 15**,** 1751.

JOUKOV, V., SORSA, T., KUMAR, V., JELTSCH, M., CLAESSON-WELSH, L., CAO, Y., SAKSELA, O., KALKKINEN, N. & ALITALO, K. 1997. Proteolytic processing regulates receptor specificity and activity of VEGF-C. *The EMBO Journal,* 16**,** 3898-3911.
KANG, H., MESQUITTA, W. T., JUNG, H. S., MOSKVIN, O. V., THOMSON, J. A. & SLUKVIN, II 2018. GATA2 Is Dispensable for Specification of Hemogenic Endothelium but Promotes Endothelial-to-Hematopoietic Transition. *Stem Cell Reports,* 11**,** 197-211.
KARKKAINEN, M. J., HAIKO, P., SAINIO, K., PARTANEN, J., TAIPALE, J., PETROVA, T. V., JELTSCH, M., JACKSON, D. G., TALIKKA, M., RAUVALA, H., BETSHOLTZ, C. & ALITALO, K. 2004. Vascular endothelial growth factor C is required for sprouting of the first lymphatic vessels from embryonic veins. *Nature Immunology,* 5**,** 74-80.
KISSA, K. & HERBOMEL, P. 2010. Blood stem cells emerge from aortic endothelium by a novel type of cell transition. *Nature,* 464**,** 112-115.
KISSA, K., MURAYAMA, E., ZAPATA, A., CORTÉS, A., PERRET, E., MACHU, C. & HERBOMEL, P. 2008. Live imaging of emerging hematopoietic stem cells and early thymus colonization. *Blood,* 111**,** 1147-1156.
KOBAYASHI, I., KOBAYASHI-SUN, J., KIM, A. D., POUGET, C., FUJITA, N., SUDA, T. & TRAVER, D. 2014. Jam1a-Jam2a interactions regulate haematopoietic stem cell fate through Notch signalling. *Nature,* 512**,** 319-323.
KOBAYASHI, I., KONDO, M., YAMAMORI, S., KOBAYASHI-SUN, J., TANIGUCHI, M., KANEMARU, K., KATAKURA, F. & TRAVER, D. 2019. Enrichment of hematopoietic stem/progenitor cells in the zebrafish kidney. *Sci Rep,* 9**,** 14205.
KOBAYASHI-OSAKI, M., OHNEDA, O., SUZUKI, N., MINEGISHI, N., YOKOMIZO, T., TAKAHASHI, S., LIM, K. C., ENGEL, J. D. & YAMAMOTO, M. 2005. GATA motifs regulate early hematopoietic lineage-specific expression of the Gata2 gene. *Mol Cell Biol,* 25**,** 7005-20.
KÜCHLER, A. M., GJINI, E., PETERSON-MADURO, J., CANCILLA, B., WOLBURG, H. & SCHULTE-MERKER, S. 2006. Development of the zebrafish lymphatic system requires VEGFC signaling. *Current biology : CB,* 16**,** 1244-1248.
KWON, H.-B., FUKUHARA, S., ASAKAWA, K., ANDO, K., KASHIWADA, T., KAWAKAMI, K., HIBI, M., KWON, Y.-G., KIM, K.-W., ALITALO, K. & MOCHIZUKI, N. 2013. The parallel growth of motoneuron axons with the dorsal aorta depends on Vegfc/Vegfr3 signaling in zebrafish. *Development (Cambridge, England),* 140**,** 4081-4090.
LANCINO, M., MAJELLO, S., HERBERT, S., DE CHAUMONT, F., TINEVEZ, J.-Y., OLIVO-MARIN, J.-C., HERBOMEL, P. & SCHMIDT, A. 2018. Anisotropic organization of circumferential actomyosin characterizes hematopoietic stem cells emergence in the zebrafish. *eLife,* 7**,** 1131.
LE GUEN, L., KARPANEN, T., SCHULTE, D., HARRIS, N. C., KOLTOWSKA, K., ROUKENS, G., BOWER, N. I., VAN IMPEL, A., STACKER, S. A., ACHEN, M. G., SCHULTE-MERKER, S. & HOGAN, B. M. 2014. Ccbe1 regulates Vegfc-mediated induction of Vegfr3 signaling during embryonic lymphangiogenesis. *Development (Cambridge, England),* 141**,** 1239-1249.
LI, L., YAN, B., SHI, Y.-Q., ZHANG, W.-Q. & WEN, Z.-L. 2012. Live imaging reveals differing roles of macrophages and neutrophils during zebrafish tail fin regeneration. *The Journal of biological chemistry,* 287**,** 25353-25360.
LIAO, E. C., PAW, B. H., OATES, A. C., PRATT, S. J., POSTLETHWAIT, J. H. & ZON, L. I. 1998. SCL/Tal-1 transcription factor acts downstream of cloche to specify hematopoietic and vascular progenitors in zebrafish. *Genes & Development,* 12**,** 621-626.
LIESCHKE, G. J., OATES, A. C., CROWHURST, M. O., WARD, A. C. & LAYTON, J. E. 2001. Morphologic and functional characterization of granulocytes and macrophages in embryonic and adult zebrafish. *Blood,* 98**,** 3087-3096.

LIN, H.-F., TRAVER, D., ZHU, H., DOOLEY, K., PAW, B. H., ZON, L. I. & HANDIN, R. I. 2005. Analysis of thrombocyte development in CD41-GFP transgenic zebrafish. *Blood,* 106**,** 3803-3810.
MATHIAS, J. R., PERRIN, B. J., LIU, T.-X., KANKI, J., LOOK, A. T. & HUTTENLOCHER, A. 2006. Resolution of inflammation by retrograde chemotaxis of neutrophils in transgenic zebrafish. *Journal of Leukocyte Biology,* 80**,** 1281-1288.
MISKOLCI, V., SQUIRRELL, J., RINDY, J., VINCENT, W., SAUER, J. D., GIBSON, A., ELICEIRI, K. W. & HUTTENLOCHER, A. 2019. Distinct inflammatory and wound healing responses to complex caudal fin injuries of larval zebrafish. *eLife,* 8**,** e45976.
MÜLLER, A. M., MEDVINSKY, A., STROUBOULIS, J., GROSVELD, F. & DZIERZAK, E. 1994. Development of hematopoietic stem cell activity in the mouse embryo. *Immunity,* 1**,** 291-301.
MURAYAMA, E., KISSA, K., ZAPATA, A., MORDELET, E., BRIOLAT, V., LIN, H.-F., HANDIN, R. I. & HERBOMEL, P. 2006. Tracing Hematopoietic Precursor Migration to Successive Hematopoietic Organs during Zebrafish Development. *Immunity,* 25**,** 963-975.
NINOV, N., BORIUS, M. & STAINIER, D. Y. 2012. Different levels of Notch signaling regulate quiescence, renewal and differentiation in pancreatic endocrine progenitors. *Development,* 139**,** 1557-67.
NORTH, T., GU, T. L., STACY, T., WANG, Q., HOWARD, L., BINDER, M., MARÍN-PADILLA, M. & SPECK, N. A. 1999. Cbfa2 is required for the formation of intra-aortic hematopoietic clusters. *Development (Cambridge, England),* 126**,** 2563-2575.
NORTH, T. E., GOESSLING, W., WALKLEY, C. R., LENGERKE, C., KOPANI, K. R., LORD, A. M., WEBER, G. J., BOWMAN, T. V., JANG, I.-H., GROSSER, T., FITZGERALD, G. A., DALEY, G. Q., ORKIN, S. H. & ZON, L. I. 2007. Prostaglandin E2 regulates vertebrate haematopoietic stem cell homeostasis. *Nature,* 447**,** 1007-1011.
OBER, E. A., OLOFSSON, B., MÄKINEN, T., JIN, S.-W., SHOJI, W., KOH, G. Y., ALITALO, K. & STAINIER, D. Y. R. 2004. Vegfc is required for vascular development and endoderm morphogenesis in zebrafish. *EMBO reports,* 5**,** 78-84.
PARDANAUD, L. & DIETERLEN-LIÈVRE, F. 1999. Manipulation of the angiopoietic/hemangiopoietic commitment in the avian embryo. *Development,* 126**,** 617-627.
PEETERS, M., OTTERSBACH, K., BOLLEROT, K., ORELIO, C., DE BRUIJN, M., WIJGERDE, M. & DZIERZAK, E. 2009. Ventral embryonic tissues and Hedgehog proteins induce early AGM hematopoietic stem cell development. *Development (Cambridge, England),* 136**,** 2613-2621.
ROSOWSKI, E. E., RAFFA, N., KNOX, B. P., GOLENBERG, N., KELLER, N. P. & HUTTENLOCHER, A. 2018. Macrophages inhibit Aspergillus fumigatus germination and neutrophil-mediated fungal killing. *PLOS Pathogens,* 14**,** e1007229.
SEITA, J., SAHOO, D., ROSSI, D. J., BHATTACHARYA, D., SERWOLD, T., INLAY, M. A., EHRLICH, L. I., FATHMAN, J. W., DILL, D. L. & WEISSMAN, I. L. 2012. Gene Expression Commons: an open platform for absolute gene expression profiling. *PLoS One,* 7**,** e40321.
SERBEDZIJA, G. N., FLYNN, E. & WILLETT, C. E. 1999. Zebrafish angiogenesis: a new model for drug screening. *Angiogenesis,* 3**,** 353-9.
SHIN, M., BEANE, T. J., QUILLIEN, A., MALE, I., ZHU, L. J. & LAWSON, N. D. 2016. Vegfa signals through ERK to promote angiogenesis, but not artery differentiation. *Development (Cambridge, England),* 143**,** 3796-3805.
SLUKVIN, I. I. 2013. Hematopoietic specification from human pluripotent stem cells: current advances and challenges toward de novo generation of hematopoietic stem cells. *Blood,* 122**,** 4035-4046.

STACKER, S. A., WILLIAMS, S. P., KARNEZIS, T., SHAYAN, R., FOX, S. B. & ACHEN, M. G. 2014. Lymphangiogenesis and lymphatic vessel remodelling in cancer. *Nat Rev Cancer,* 14**,** 159-72.
STUART, T., BUTLER, A., HOFFMAN, P., HAFEMEISTER, C., PAPALEXI, E., MAUCK, W. M., III, HAO, Y., STOECKIUS, M., SMIBERT, P. & SATIJA, R. 2019. Comprehensive Integration of Single-Cell Data. *Cell,* 177**,** 1888-1902.e21.
SUKBUNTHERNG, J., CROPP, G., HANNAH, A., WAGNER, G. S., SHAWVER, L. K. & ANTONIAN, L. 2001. Pharmacokinetics and interspecies scaling of a novel VEGF receptor inhibitor, SU5416. *J Pharm Pharmacol,* 53**,** 1629-36.
SWIRSKY, D. & BAIN, B. J. 2006. Chapter 13 - Erythrocyte and leucocyte cytochemistry. *In:* LEWIS, S. M., BAIN, B. J. & BATES, I. (eds.) *Dacie and Lewis Practical Haematology (Tenth Edition).* Philadelphia: Churchill Livingstone.
TAMPLIN, O. J., DURAND, E. M., CARR, L. A., CHILDS, S. J., HAGEDORN, E. J., LI, P., YZAGUIRRE, A. D., SPECK, N. A. & ZON, L. I. 2015. Hematopoietic Stem Cell Arrival Triggers Dynamic Remodeling of the Perivascular Niche. *Cell,* 160**,** 241-252.
THISSE, C. & THISSE, B. 2008. High-resolution in situ hybridization to whole-mount zebrafish embryos. *Nature Protocols,* 3**,** 59-69.
VILLEFRANC, J. A., NICOLI, S., BENTLEY, K., JELTSCH, M., ZARKADA, G., MOORE, J. C., GERHARDT, H., ALITALO, K. & LAWSON, N. D. 2013. A truncation allele in vascular endothelial growth factor c reveals distinct modes of signaling during lymphatic and vascular development. *Development (Cambridge, England),* 140**,** 1497-1506.
VOGRIN, A. J., BOWER, N. I., GUNZBURG, M. J., ROUFAIL, S., OKUDA, K. S., PATERSON, S., HEADEY, S. J., STACKER, S. A., HOGAN, B. M. & ACHEN, M. G. 2019. Evolutionary Differences in the Vegf/Vegfr Code Reveal Organotypic Roles for the Endothelial Cell Receptor Kdr in Developmental Lymphangiogenesis. *Cell Rep,* 28**,** 2023-2036 e4.
WANG, G., MUHL, L., PADBERG, Y., DUPONT, L., PETERSON-MADURO, J., STEHLING, M., LE NOBLE, F., COLIGE, A., BETSHOLTZ, C., SCHULTE-MERKER, S. & VAN IMPEL, A. 2020. Specific fibroblast subpopulations and neuronal structures provide local sources of Vegfc-processing components during zebrafish lymphangiogenesis. *Nat Commun,* 11**,** 2724.
WESTERFIELD, M. 2000. *The Zebrafish Book. A Guide for the Laboratory Use of Zebrafish (Danio rerio),* Eugene, OR, University of Oregon Press.
WILLETT, C. E., ZAPATA, A. G., HOPKINS, N. & STEINER, L. A. 1997. Expression of ZebrafishragGenes during Early Development Identifies the Thymus. *Developmental Biology,* 182**,** 331-341.
YOKOMIZO, T. & DZIERZAK, E. 2010. Three-dimensional cartography of hematopoietic clusters in the vasculature of whole mouse embryos. *Development (Cambridge, England),* 137**,** 3651-3661.
ZHU, Q., GAO, P., TOBER, J., BENNETT, L., CHEN, C., UZUN, Y., LI, Y., HOWELL, E. D., MUMAU, M., YU, W., HE, B., SPECK, N. A. & TAN, K. 2020. Developmental trajectory of prehematopoietic stem cell formation from endothelium. *Blood,* 136**,** 845-856.
ZOU, Z., ENIS, D. R., BUI, H., KHANDROS, E., KUMAR, V., JAKUS, Z., THOM, C., YANG, Y., DHILLON, V., CHEN, M., LU, M., WEISS, M. J. & KAHN, M. L. 2013. The secreted lymphangiogenic factor CCBE1 is essential for fetal liver erythropoiesis. *Blood,* 121**,** 3228-3236.

Figures

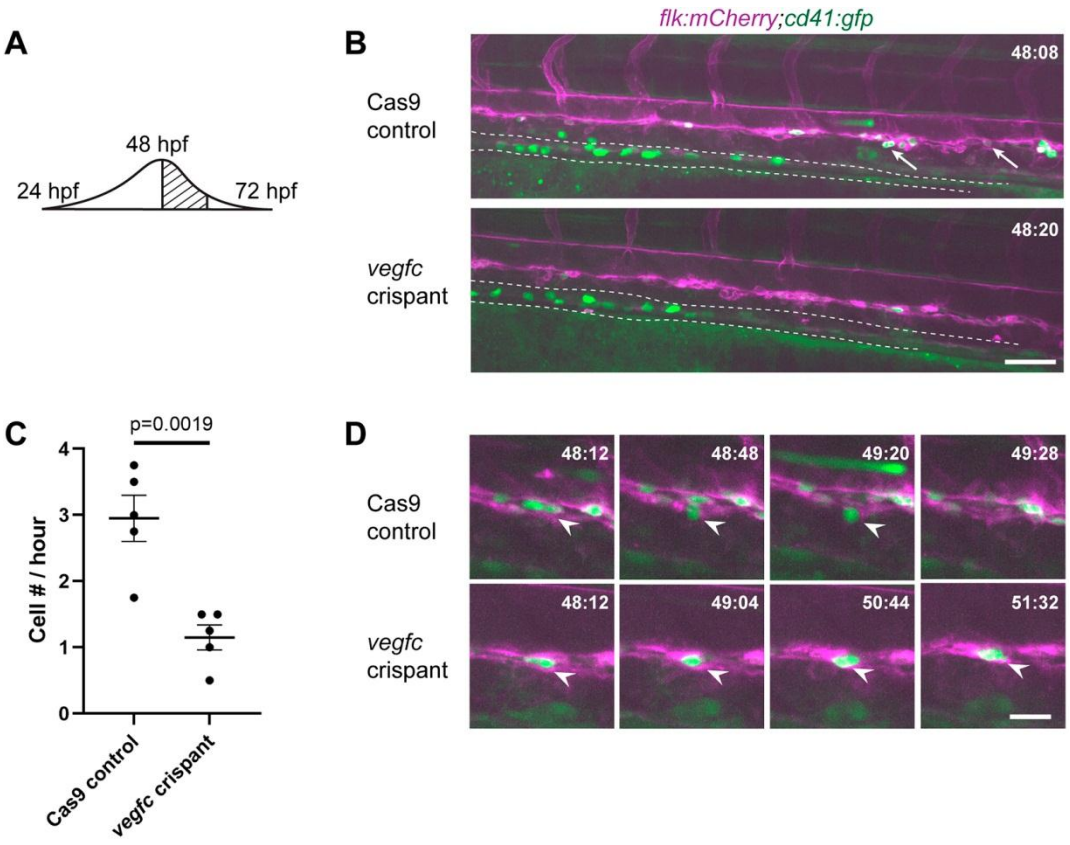

Figure 1. *vegfc* loss-of-function results in decreased HSPC emergence from the DA.

(A) Schematic showing the wave of emergence from the DA; this experiment occurs during the peak. (B) Single frame of time-lapse (hours post fertilization:min) showing *cd41:gfp*+ (green) HSPCs (arrows) budding from *flk:mCherry*+ (magenta) HE in Cas9 control (top panel) or *vegfc* crispant embryos (bottom panel). White arrows indicate cells undergoing EHT. Dotted line outlines developing pronephric tubules (see Movies 1 and 2) (C) Quantification of the total number of *cd41:gfp*+ HSPCs budding from the DA between 48 and 52 hpf, divided by 4 to give cell # per hour. n=5 embryos per condition, p=0.0019. (D) 4 frames selected from Cas9 control and *vegfc* crispant time-lapse movies depicting HSPC budding (top panels) and static hammock-like cell (bottom panels). White arrow heads indicate the cell of interest. Scale bars: (B) 50 µm; (D) 10 µm. Error bars show mean ± SEM.

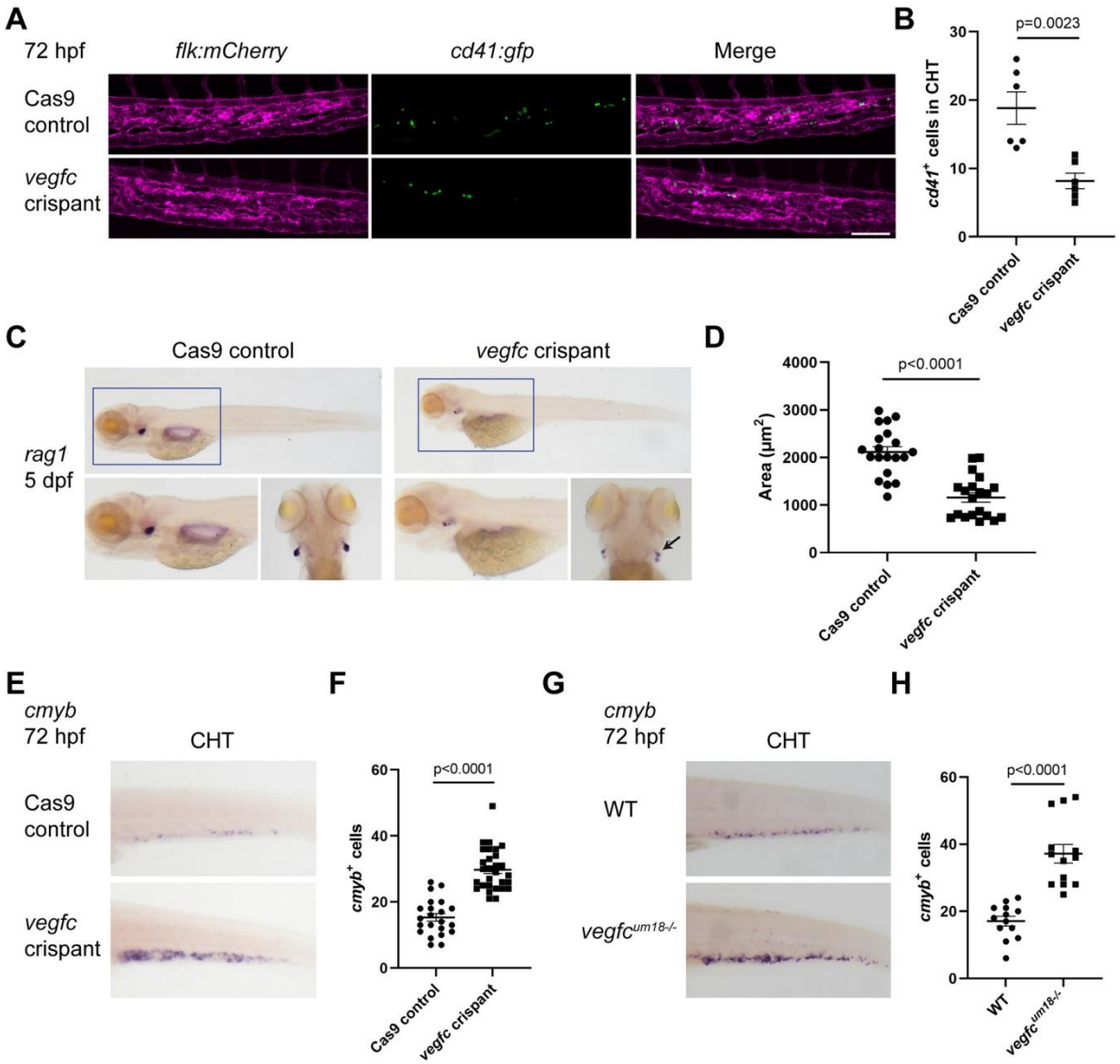

Figure 2. *vegfc* loss-of-function leads to altered definitive hematopoiesis throughout development.

(A) *In vivo* imaging of *cd41:gfp*(green)*/flk:mCherry*(magenta) depicting decreased HSPC numbers in the CHT of *vegfc* loss-of-function embryos at 72 hpf. HSPCs are green and vessels are magenta(B) Quantification of *cd41:gfp*$^{+}$ cells within the CHT, as shown in (A); Cas9 control versus *vegfc* crispants, p=0.0023. (C) *vegfc* crispants show decreased area of *rag1* expression in the thymus at 5 dpf. Black arrow highlights area of *rag1* staining in *vegfc* crispant. (D) Quantification of the area of *rag1* expression, p<0.0001. (E) *vegfc* loss-of-function increases the number of *cmyb* expressing cells in the CHT compared to Cas9 control embryos. (F)

Quantification of the number of *cmyb* expressing cells in the CHT at 72 hpf, $p<0.0001$. (G) *vegfc*$^{um18-/-}$ mutant embryos show an increased number of *cmyb* expressing cells in the CHT at 72 hpf. (H) Number of *cmyb* expressing cells in the CHT at 72 hpf, $p<0.0001$. Scale bar: (A) 40 µm. Error bars show mean ± SEM.

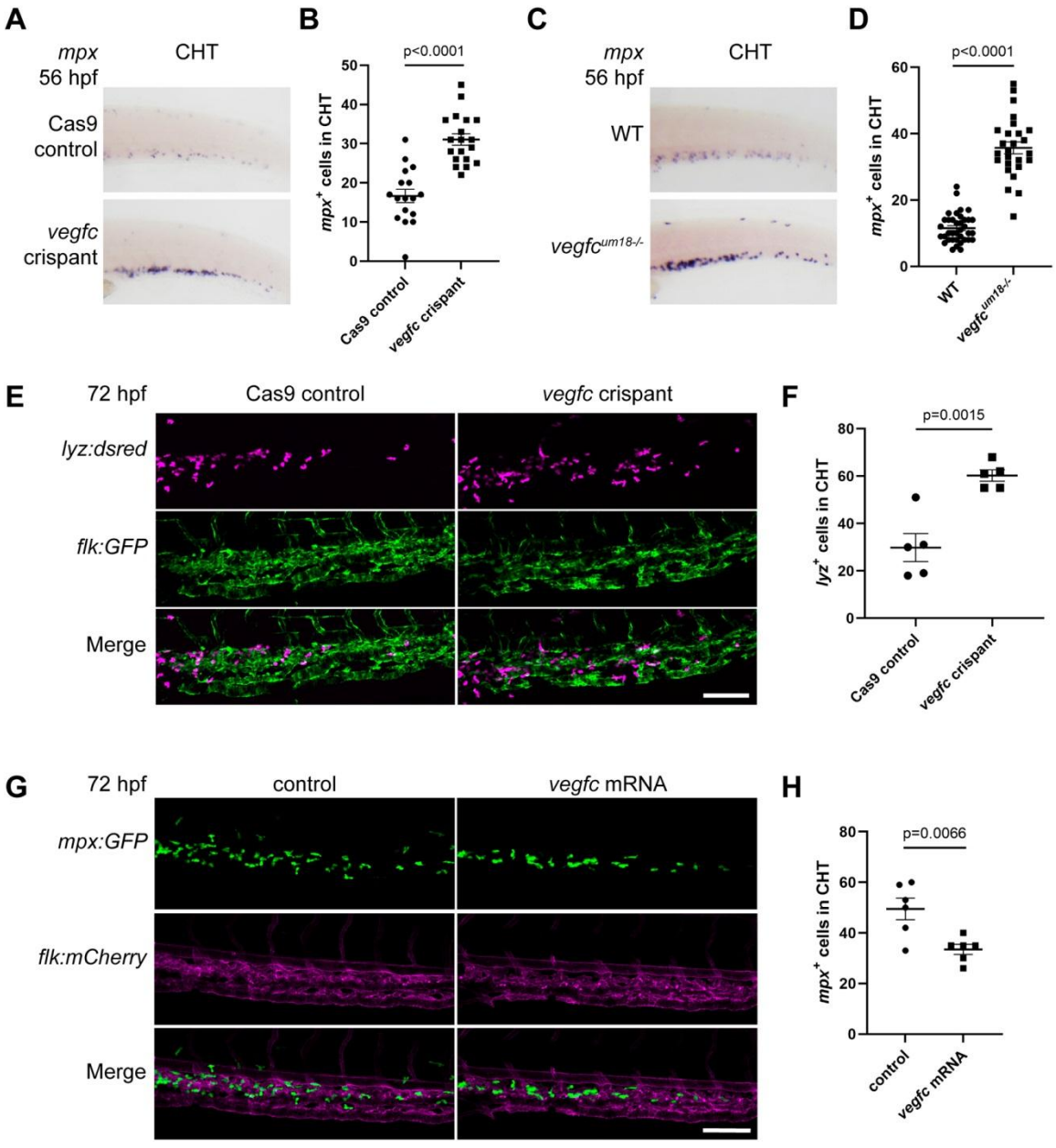

Figure 3. *vegfc* loss-of-function embryos display an increase in myeloid cells in the CHT.

(A) *vegfc* loss-of-function increases the number of *mpx* expressing cells in the CHT region at 56 hpf. (B) Quantification of the number of *mpx* expressing cells in the CHT at 56 hpf, p<0.0001. (C) *vegfc*$^{um18-/-}$ mutant embryos show increased *mpx* expression in the CHT at 56 hpf. (D) Quantification of the number of *mpx* expressing cells in the CHT at 72 hpf, p<0.0001. (E) *vegfc* loss-of-function increases the number of *lyz:DsRed2*+ (magenta) cells in the CHT at 72 hpf. *flk:gfp*+ vessels are green. (F) Quantification of *lyz:DsRed2*+ cells within the CHT, p=0.0015.

(G) Overexpression of *vegfc* decreases the number of *mpx:gfp*+ (green) cells in the CHT at 72 hpf. *flk:mCherry*+ vessels are magenta. (H) Quantification of the number of *mpx* expressing cells in the CHT at 72 hpf, p=0.0066. Scale bars: 50 µm. Error bars show mean ± SEM.

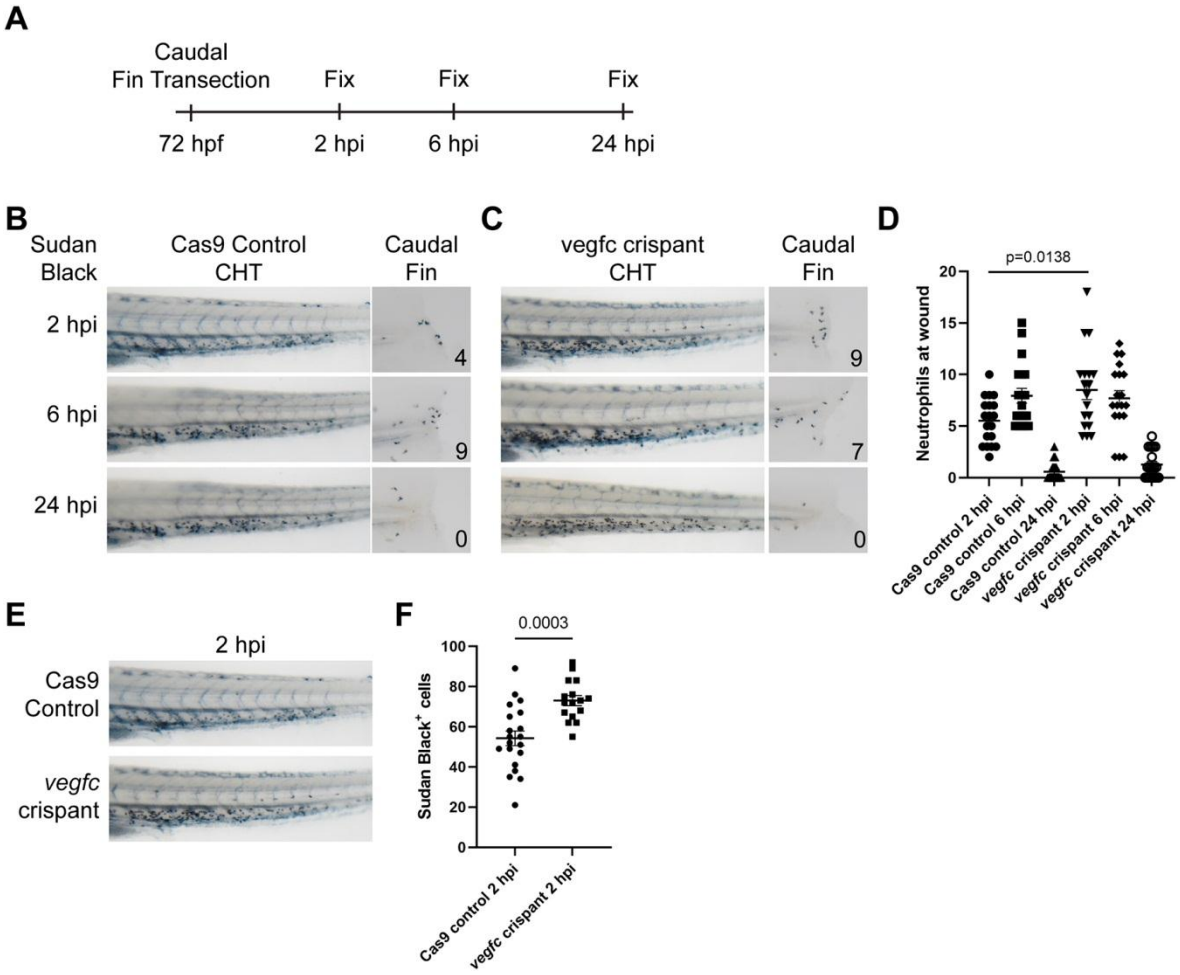

Figure 4. *vegfc* loss-of-function embryos show altered injury response.

(A) Experimental approach. Caudal fins were transected distally without injury of the notochord at 72 hpf. Embryos were fixed in 4% PFA at different intervals following transection. (B) Brightview images of Sudan black staining in Cas9 control embryos depicting neutrophil response at 2, 6 and 24 hpi. Neutrophil response peaks at 6 hpi and subsides by 24 hpi. (C) Brightview images of Sudan black staining in *vegfc* loss-of-function embryos. Neutrophil response peaks at 2 hpi and diminishes over time. (D) Quantification of neutrophil number within the injury area, p=0.0138. (E) Representative images showing increased neutrophils within the CHT of *vegfc* loss-of-function embryos at 2 hpi. (F) Quantification of the number of Sudan Black positive neutrophils within the CHT at 2 hpi, p= 0.0003. Error bars show mean ± SEM.

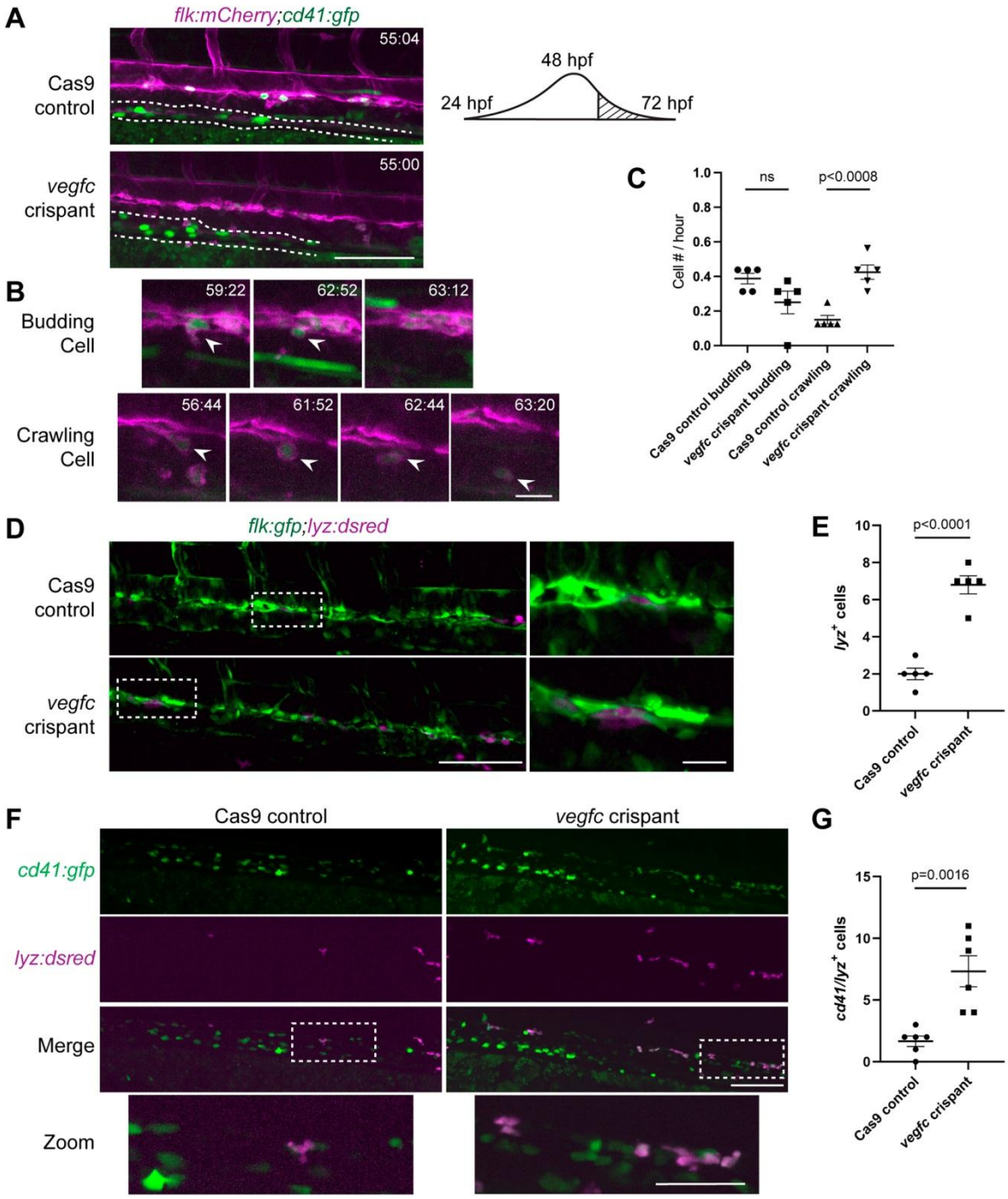

Figure 5. Late-stage hemogenic endothelium in *vegfc* loss-of-function embryos gives rise to increased crawling myeloid-like cells.

(A) Single frames of *cd41:gfp*+(green)/*flk:mCherry*+(magenta) time-lapse (hours post fertilization:minutes) showing the overall difference in DA morphology between Cas9 controls

(top panel) and *vegfc* crispants (bottom panel). The dotted line outlines the pronephric tubules. A schematic showing the time window of imaging for this experiment that is past the peak of HSPC emergence form the DA. (B) 3 frames selected from Cas9 control time-lapse movie (Movie 3) between 56-72 depicting HSPC budding. 4 frames selected from *vegfc* crispant time-lapse movie (Movie 4) depicting HSPC crawling. White arrow heads indicate the cell of interest. (C) Quantification of *cd41:gfp+/flk:mCherry+* cell behavior within the DA, $p<0.0008$. The total number of events observed are divided by the duration of the experiment (16 hours) to give the number of events per hour. The data shown is from one experiment with a total of n=5 control and n=5 vegfc crispant embryos. (D) Single frames of *flk:gfp+*(green)*/lyz:DsRed2+*(magenta) time-lapse (hours post fertilization:minutes) showing the overall number of *lyz:DsRed2+* cells within the DA of Cas9 controls (top panel) and *vegfc* crispants (bottom panel). The dotted line outlines the zoomed region. (E) Quantification of the number of resident *lyz:DsRed2*$^{+}$ cells within the ventral wall of the DA, $p<0.0001$. (F) *vegfc* crispants show increased *cd41:gfp+*(green)*/lyz:DsRed2+*(magenta) cells in the DA at 56 hpf. Bottom panel shows zoomed image of double positive cells. (G) Quantification of the number of *cd41:gfp+/lyz:DsRed2+* cells within the DA, $p=0.0016$. Scale bar: (A) 40 μm; (B) 10 μm; (D) 100 μm, 10 μm; (F) 100 μm, 50 μm. Error bars show mean ± SEM.

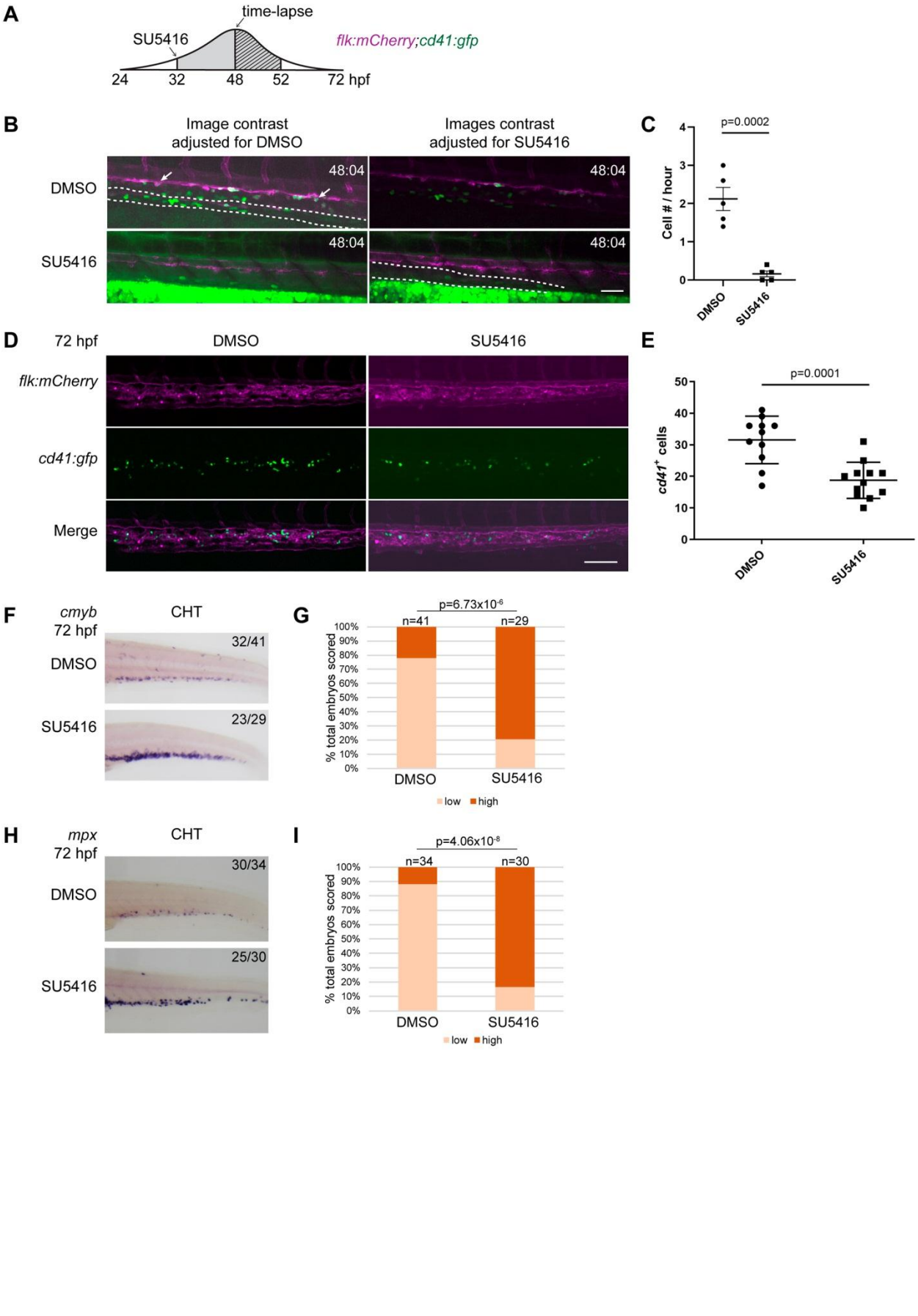

Figure 6. Chemical inhibition of vegf family receptors phenocopies *vegfc* loss-of-function.

(A) Experimental schematic showing SU5416 dosage starting at 32 hpf, followed by time-lapse imaging from 48 to 52 hpf. The hatched area indicates the time-lapse window, and the grey area indicates the time of SU5416 treatment. (B) Treatment of embryos with SU5416 created high levels of autofluorescence in the yolk sac. Therefore, we present images with levels (brightness and contrast) optimized for GFP signal in DMSO-treated control embryos (left column), and SU5416-treated embryos (right column). Single frames of the time-lapse (hours post fertilization:min) show *cd41:gfp*+ HSPCs (green) budding from the *flk:mCherry*+ DA (magenta). White arrows indicate cells undergoing EHT. Compared to DMSO controls (top panels), there are very few budding HSPCs in SU5416-treated embryos (bottom panels). Dotted lines outline pronephric tubules. (C) Quantification of the total number of *cd41:gfp*+ HSPCs budding from the DA between 48 and 52 hpf. The total number of events observed are divided by the duration of the experiment (4 hours) to give the number of events per hour. The data shown is from one experiment with n=5 DMSO and n=5 SU5416-treated embryos. p=0.0002. (D) *In vivo* imaging of the CHT in *cd41:gfp/flk:mCherry* embryos at 72 hpf, after treatment with SU5416 from 32 hpf, shows a reduction in HSPC numbers. (E) Quantification of *cd41:gfp*+ cells within the CHT, as shown in (D); DMSO control (n=11) versus SU5416-treated (n=12). p=0.0001. (F) Treatment with SU5416 increases the percentage of embryos with high *cmyb* expression compared to DMSO-treated embryos. *cmyb* expression was scored in the CHT at 72 hpf. (G) Percentage of total embryos scored and classified as having low or high *cmyb* expression, $p=6.73x10^{-6}$. (H) Treatment with SU5416 increases the percentage of embryos with high *mpx* expression compared to DMSO controls. (I) Percentage of total embryos scored and classified as having low or high *mpx* expression, $p=4.06x10^{-8}$. SU5416 dose is 0.75 μM in DMSO. Scale bar = 50μm.

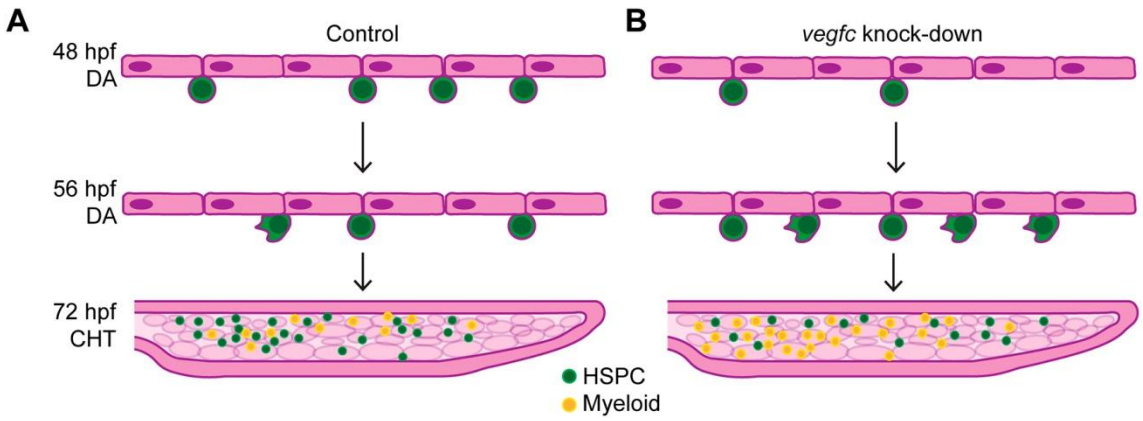

Figure 7. Model of vegfc function in determining HE fate decisions in the DA.

(A) Schematic of HSPC development in control embryos. Emergence of nascent HSPCs from the DA peaks at 48 hpf. In late stage EHT (56 hpf and later) there is a decrease in HSPC emergence and the appearance of few crawling cells. HSPCs then colonize the CHT, where there are also myeloid cells present. (B) Schematic of HSPC development in *vegfc* loss-of-function embryos. There are significantly less HSPCs during the peak of emergence from the DA. In late stage EHT there is a change in cell behavior and many crawling cells emerge from the DA. In the CHT there are decreased HSPCs and an increased number of myeloid cells.

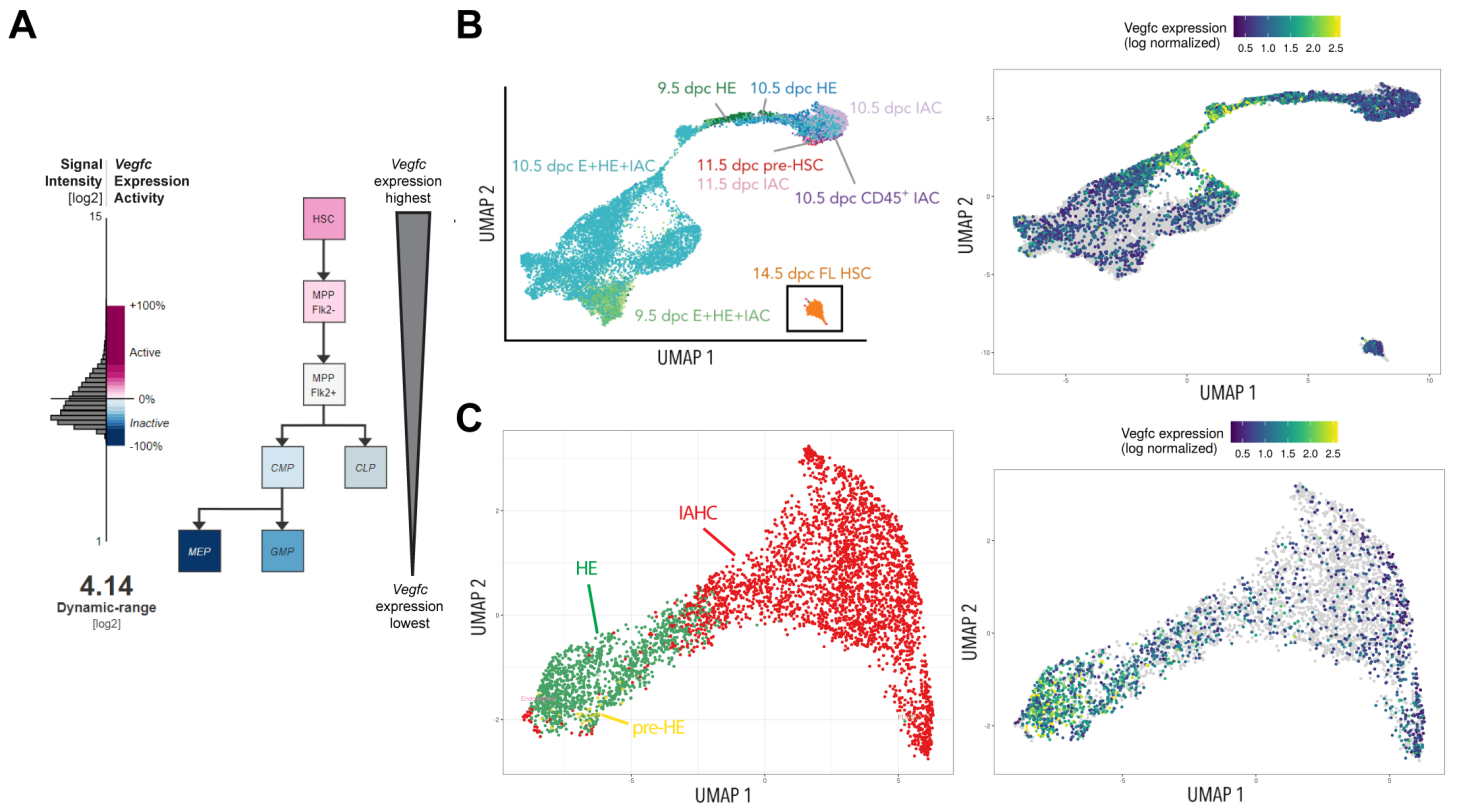

Fig. S1. Published gene expression data shows VEGFC is expressed in mouse HSPCs and HE and zebrafish HSPCs.

(A) Microarray gene expression data from sorted mouse hematopoietic populations shows *Vegfc* is most highly expressed in undifferentiated HSPCs (pink) and is down-regulated in more differentiated progenitors (blue) (Seita et al., 2012, Gazit et al., 2013). (B) UMAP plot of mouse EHT using scRNA-seq data. Expression of *Vegfc* within the pre-HE and HE populations (Zhu et al., 2020). (C) Detailed UMAP of HE to intra-aortic clusters (IAC) and expression of *Vegfc* within the HE population.

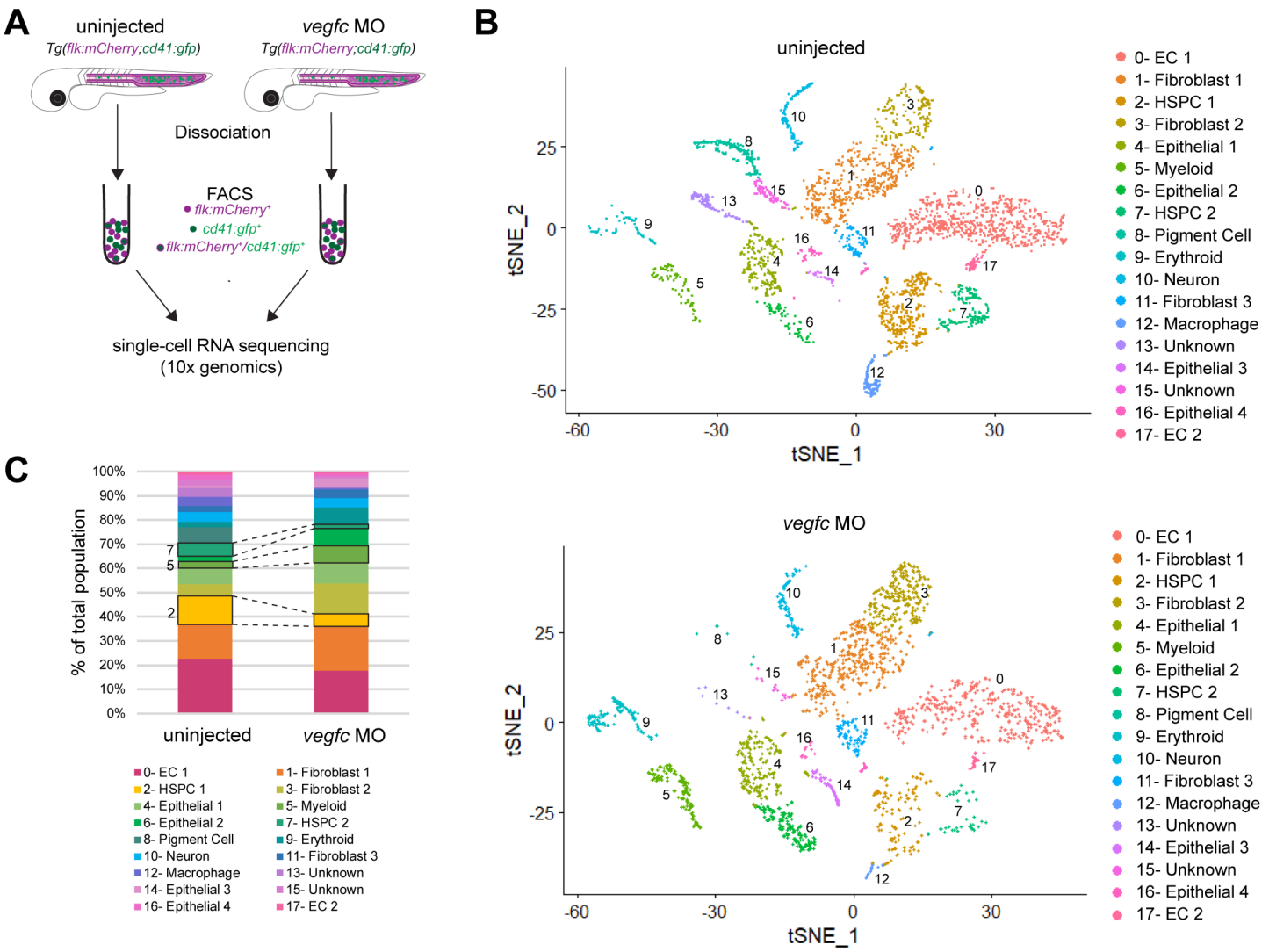

Fig. S2. Single-cell resolution map of 52 hpf zebrafish.

(A) Schematic of scRNA-seq experimental design. (B) t-SNE clustering map of 3,442 single cells from uninjected and 2,213 single cells from *vegfc* morphant embryos at 52 hpf. (C) Percentage of cells in each cluster uninjected vs *vegfc* MO. Dotted lines depict cluster size changes of interest. Raw and processed scRNA-seq data has been deposited in the NCBI GEO database (GSE186565).

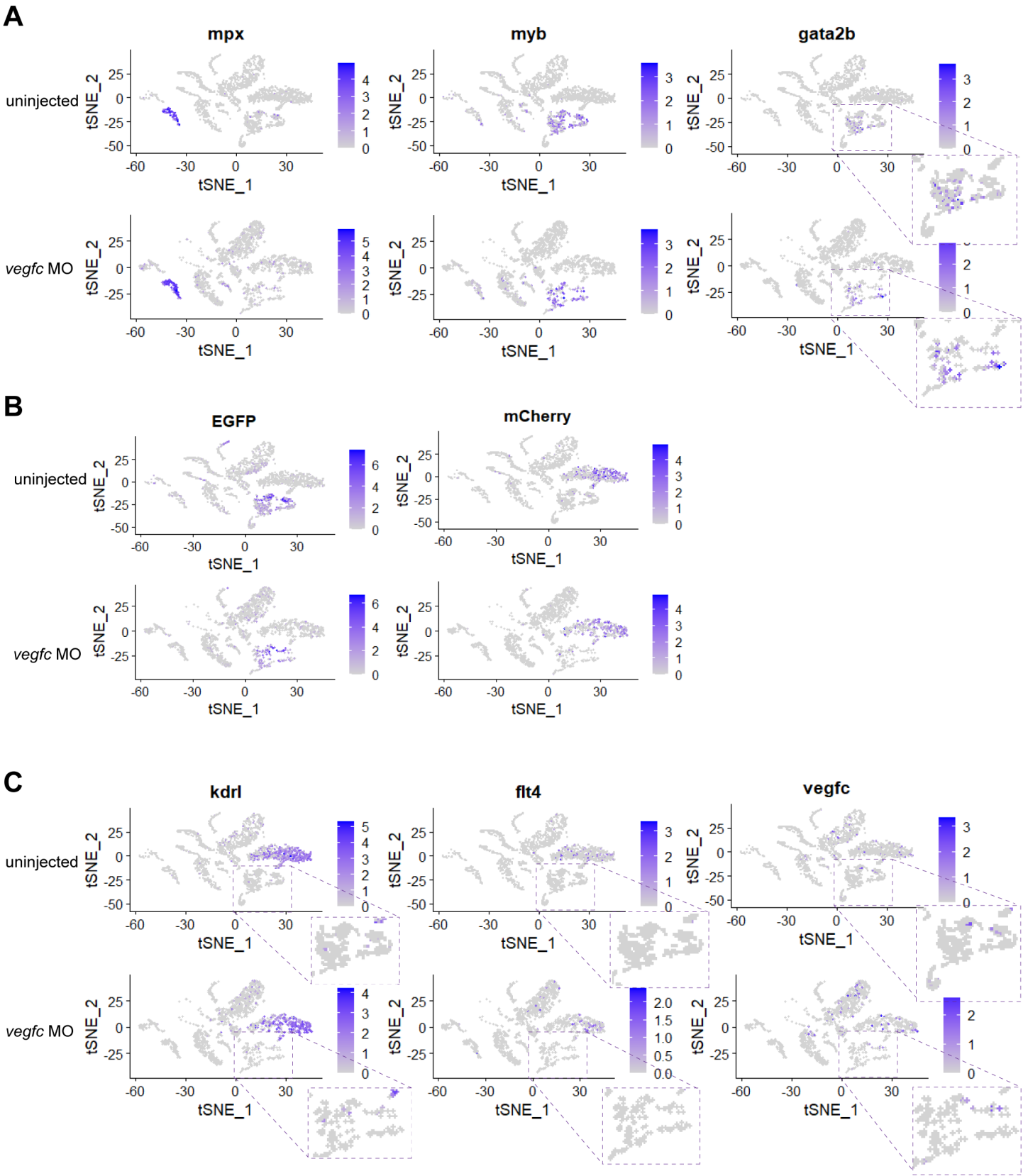

Fig. S3. *vegfc* and its receptors are expressed in HSPCs and ECs at 52 hpf.

(A) Identification of hematopoietic populations using known genetic markers: myeloid cells (*mpx*); HSPCs (*myb*, *gata2b*). (B) Confirmation of HSPC and EC clusters using expression of transgenic lines *cd41:gfp* and *flk:mCherry*. (C) Expression of *vegfc* and its receptors *kdrl/vegfr2a* and *flt4/vegfr3*.

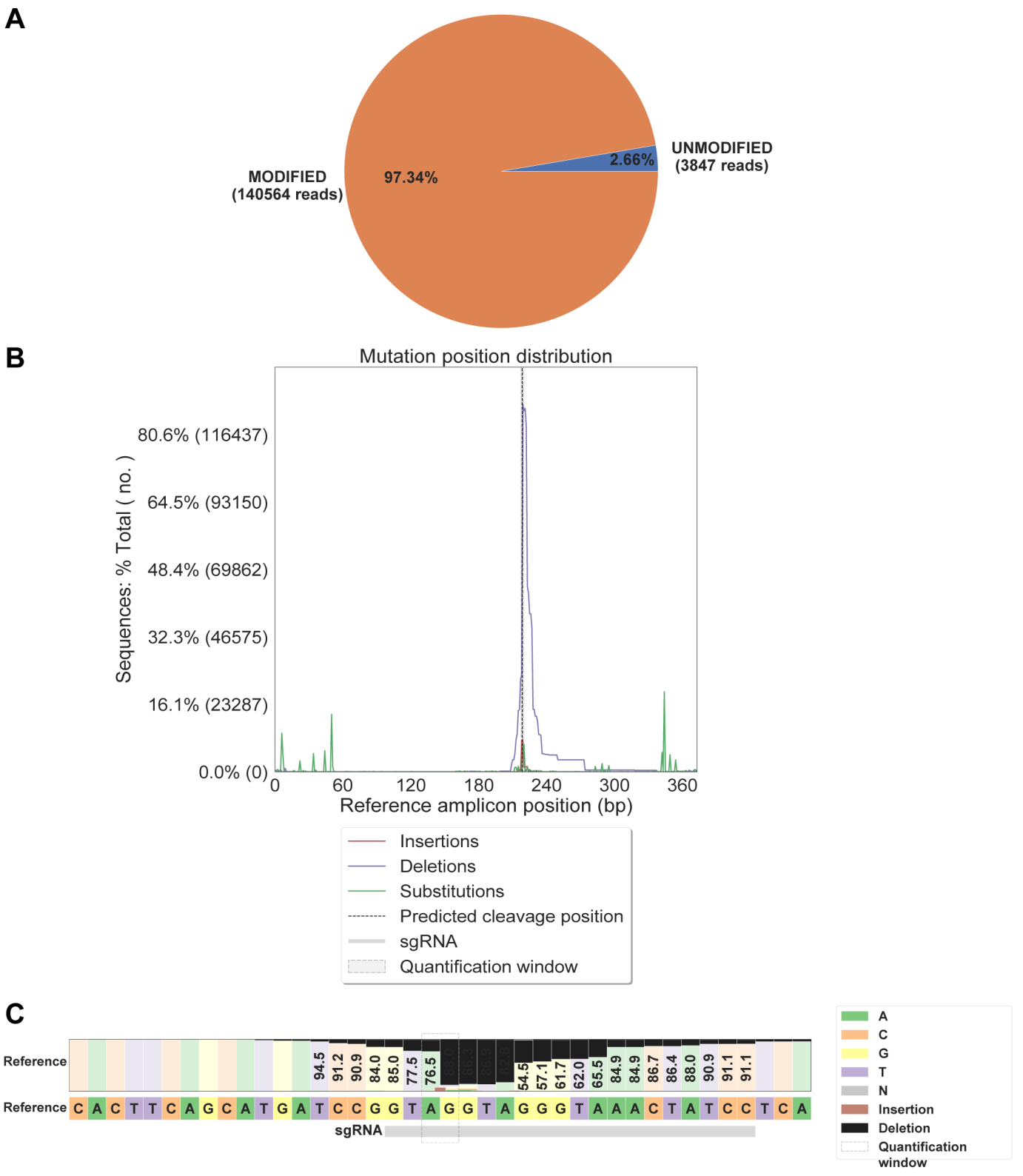

Fig. S4. Efficiency of *vegfc* CRISPR/Cas9 reagents in pooled F0 embryos.

Genomic DNA was extracted from a minimum of 15 embryos injected with *vegfc* RNP (Burger et al., 2016), followed by Illumina MiSeq sequencing and CRISPResso2 analysis (Clement et al., 2019). (A) Alignment and editing frequency of reads as determined by the percentage and number of sequence reads showing modified alleles. Our *vegfc* gRNA sequence shows a 97.34% modification rate. (B) Frequency of insertions (red), deletions (purple), and substitutions (green) across the amplicon. *vegfc* gRNA sequence showed high rate of deletion around the quantification window. (C) Nucleotide distribution around the *vegfc* sgRNA sequence GTAGGTAGGGTAAACTATCC.

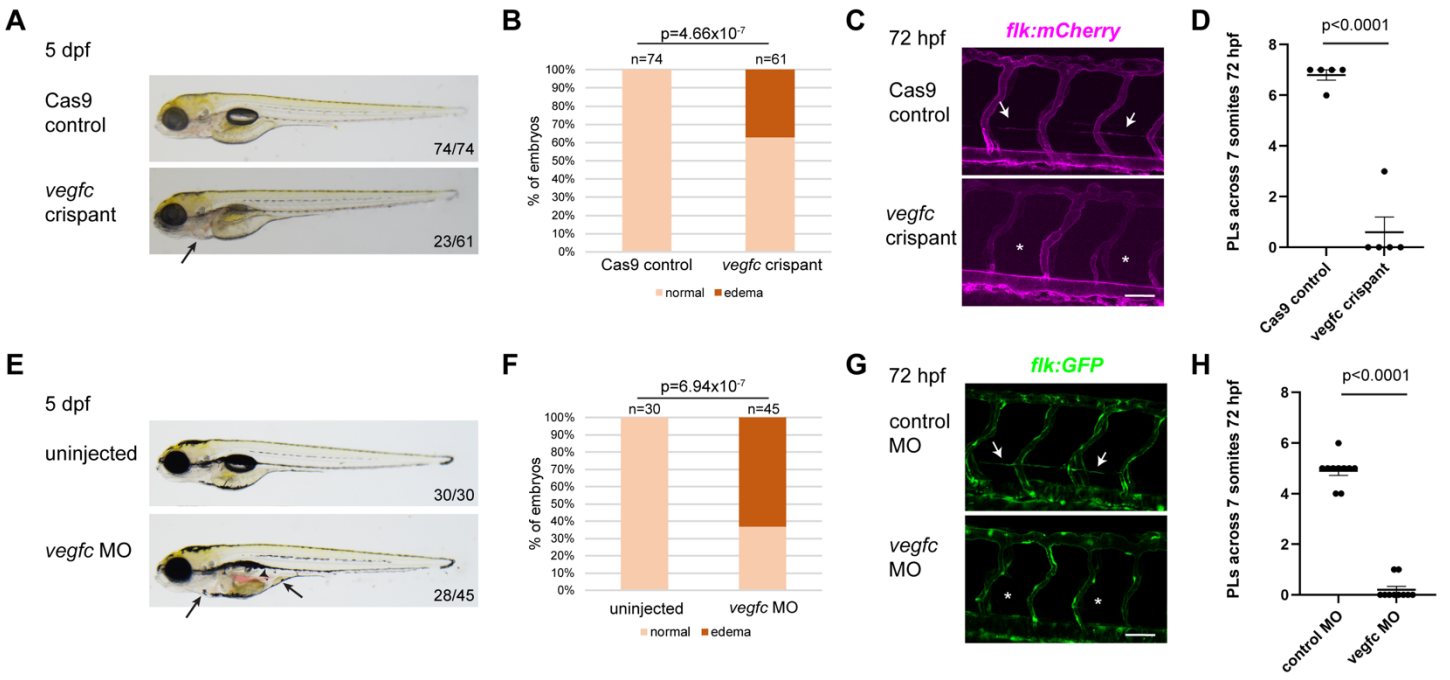

Fig. S5. *vegfc* crispants and morphants phenocopy lymphatic defects in *vegfc* mutants.

(A) Representative images of 5 dpf Cas9 control and *vegfc* crispant embryos. The black arrow indicates area of cardiac edema. All control embryos displayed normal morphology (73/73), whereas *vegfc* crispants exhibited edema (23/61). (B) Quantification of embryos shows a significant number of *vegfc* crispants have edema ($p = 4.66x10^{-7}$). (C) Parachordal lymphangioblasts (PLs) are absent from the horizontal myoseptum in *flk:mCherry vegfc* crispants (asterisk), as compared with Cas9 control injected siblings at 72 hpf (arrows indicate PLs). (D) Quantification of PLs counted across 7 somites at 72 hpf in control (n=5) and *vegfc* crispant (n=5) embryos. PLs are significantly reduced in *vegfc* crispants ($p < 0.0001$). (E) Representative images of 5 dpf uninjected and *vegfc* morphant embryos. The anterior black arrow indicates an area of cardiac edema, and the posterior black arrow indicates gut edema. The black arrowhead indicates blood pooling. All uninjected embryos (30/30) in this experiment, and previously injected control morphants (data not shown), displayed normal morphology at 5 dpf. Conversely, vegfc morphants exhibited edema and blood pooling (28/45). (F) Quantification of embryos shows a significant number of *vegfc* morphants have edema ($p = 6.94x10^{-7}$). (G) PLs are absent from the horizontal myoseptum in *flk:GFP vegfc* morphants (asterisk), as compared with control morphants at 72 hpf (arrows indicate PLs). (H) Quantification of PLs counted across 7 somites at 72 hpf in control (n=10) and *vegfc* morphant (n=10) embryos. PLs are significantly reduced in *vegfc* morphants ($p < 0.0001$). Scale bars: 50 μm.

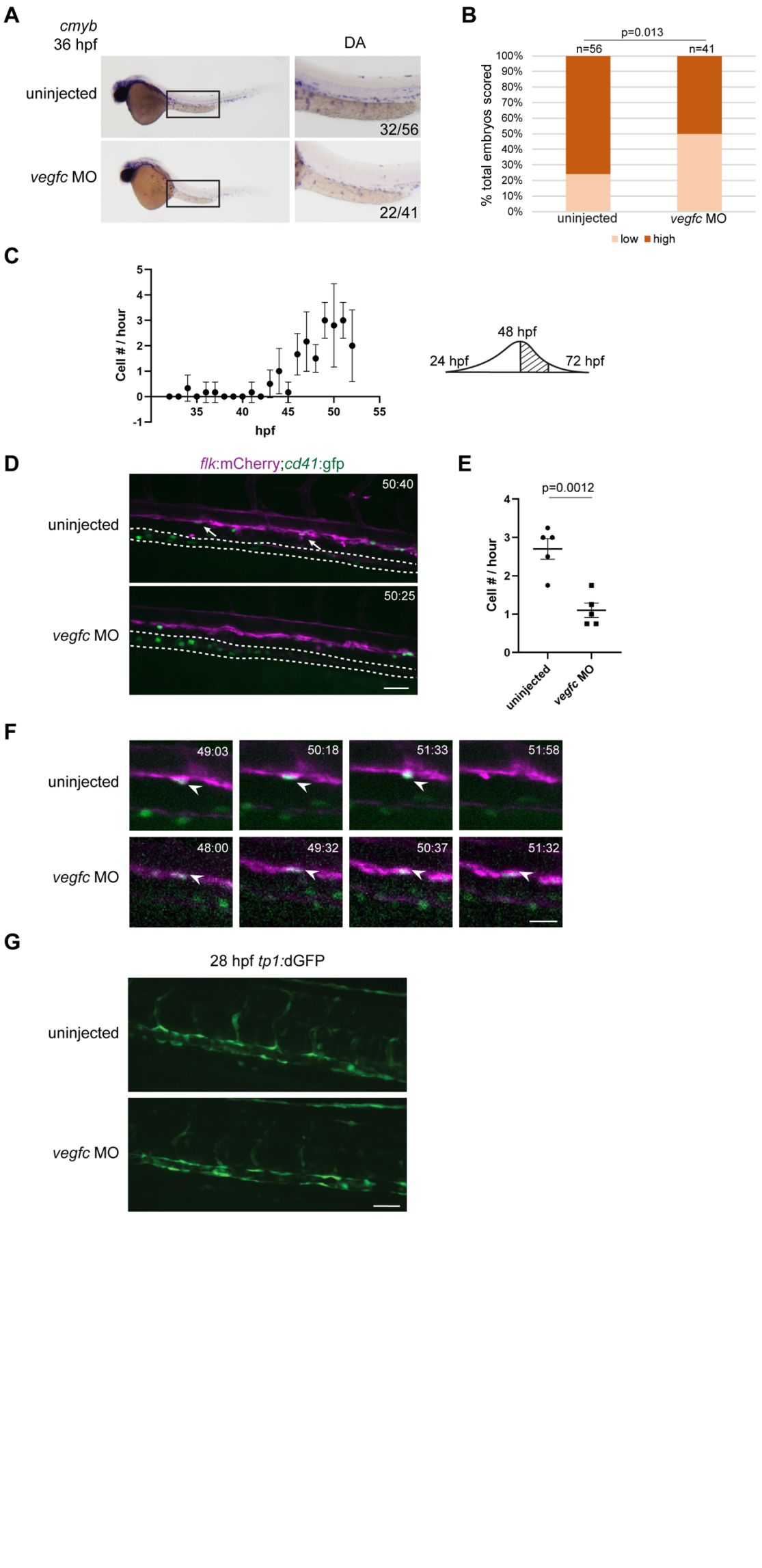

Fig. S6. *vegfc* morphants have decreased HSPC emergence from the DA.

(A) *cmyb* expression in the DA at 36 hpf in *vegfc* morphants and uninjected controls. (B) Percentage of embryos scored and classified as having low or high *cmyb* expression, p=0.013. (C) Quantification of *cd41:gfp*+ HSPC emergence (Cell # / hour) from *flk:mCherry*+ HE per hour from 32-52 hpf. n=12 embryos. Schematic showing the wave of emergence from the DA. The experiment below begins from the peak of emergence at 48 hpf (hatched region). (D) Single frame of time-lapse (hours post fertilization:min) showing *cd41:gfp*+ HSPCs (arrows, green) budding from *flk:mCherry*+ HE (violet) in uninjected (top panel) or *vegfc* MO embryos (bottom panel). White arrows indicate cells undergoing EHT. Dotted line outlines developing pronephric tubules. (E) Quantification of the total number of *cd41:gfp*+ HSPCs budding from the DA between 48 and 52 hpf, divided by 4 to give cell # per hour. p=0.0012. (F) 4 frames selected from uninjected and *vegfc* MO time-lapse movies depicting HSPC budding (top panels) and static hammock cell (bottom panels). White arrow heads indicate the cell of interest. (G) Specification of the DA and notch activity is unchanged in *vegfc* MO embryos. Representative images of *tp1:dGFP* expression in uninjected and *vegfc* MO embryos at 28 hpf (n=8 embryos per treatment group). Scale bars: (D,G) 50 μm; (F) 10 μm. Error bars show mean ± SEM.

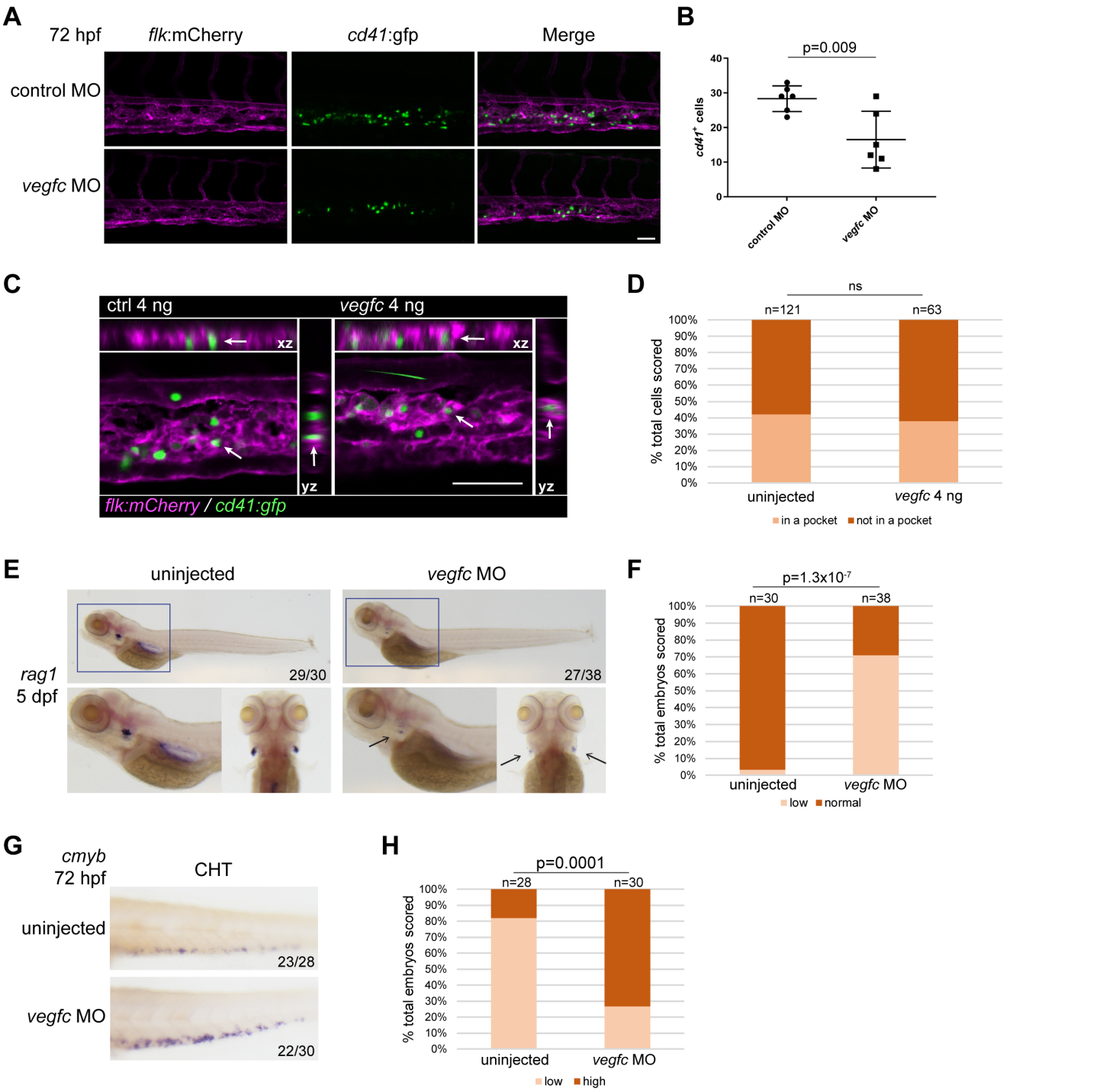

Fig. S7. *vegfc* loss-of-function leads to altered definitive hematopoiesis throughout development.

(A) *In vivo* imaging of *cd41:gfp/flk:mCherry* depicting decreased HSPC numbers in the CHT of *vegfc* loss-of-function embryos at 72 hpf. (B) Quantification of *cd41:gfp*$^{+}$ cells within the CHT, as shown in (A); control versus *vegfc* morphants, p=0.0093. (C) Representative images of *cd41:gfp/flk:mCherry* embryos in xy, xz, yz planes showing HSPCs surrounded by ECs in the CHT at 72 hpf of control and *vegfc* morphant embryos. CHT remodeling is not impaired in *vegfc* morphants. (D) There is no significant difference in the percentage of individual *cd41:gfp*+ cells within a *flk:mCherry*+ EC pocket between control embryos (n=121) or vegfc morphants (n=63). (E) *vegfc* morphants show decreased *rag1* expression in the thymus at 5 dpf. Black arrow highlights area of *rag1* staining in *vegfc* morphant. (F) Percentage of total embryos scored, classified as having low or normal *rag1* expression, p=1.3x10^{-7}. Scale bar: 40 μm. (G) *vegfc* loss-of-function increases the percentage of embryos with high *cmyb* expression compared to uninjected embryos. *cmyb* expression was scored in the CHT at 72 hpf. (H) Percentage of total embryos scored and classified as having low or high *cmyb* expression, p=0.0001. Error bars show mean ± SEM.

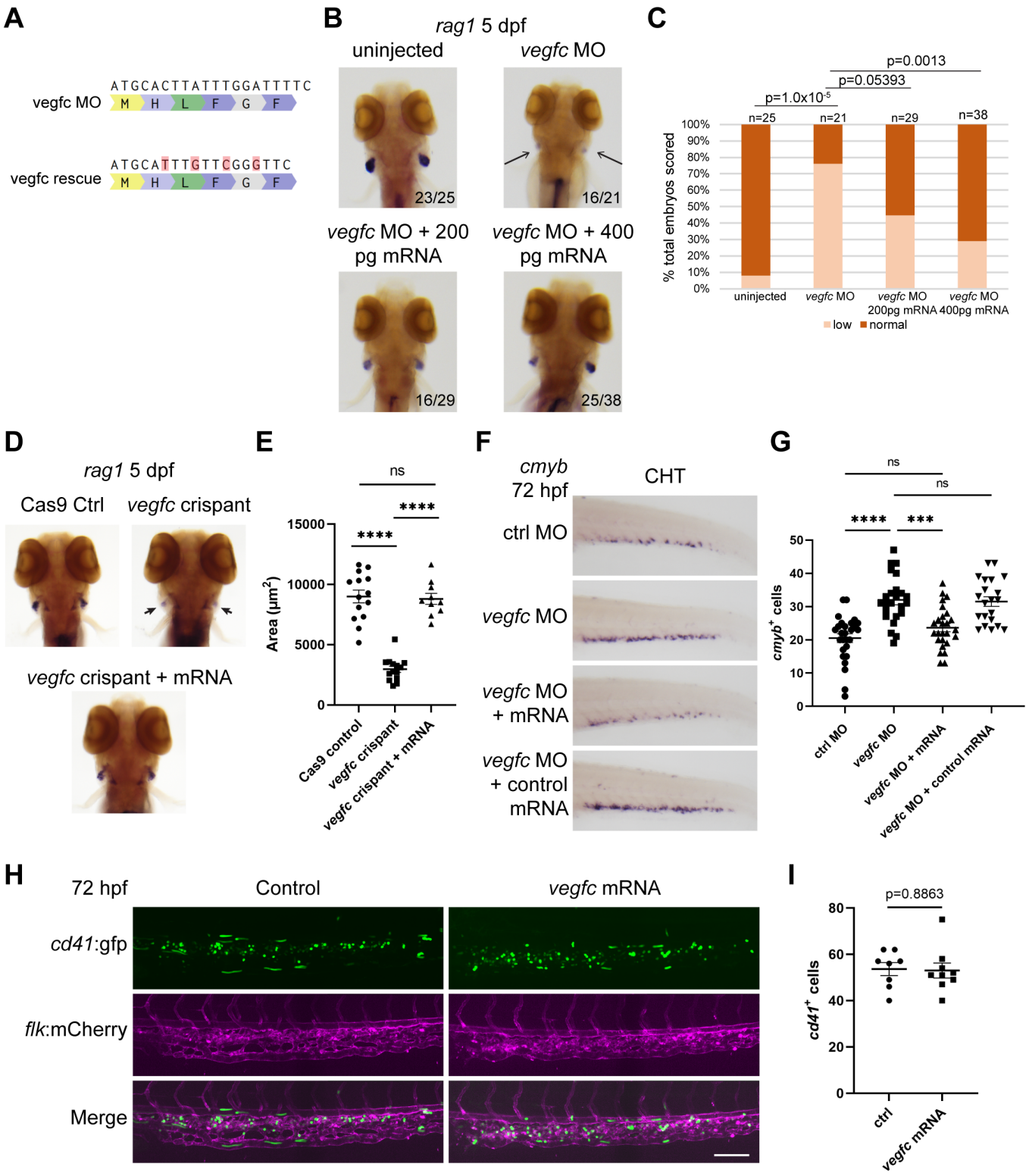

Fig. S8. MO resistant *vegfc* mRNA rescues impaired definitive hematopoiesis.

(A) Schematic showing the *vegfc* MO target sequence with corresponding amino acids and the MO-resistant rescue mRNA with altered base pairs highlighted in red. Corresponding amino acid sequence remains the same as endogenous vegfc. (B) *vegfc* morphants show decreased *rag1* expression in the thymus at 5 dpf. Injection of 200 pg rescue mRNA trends toward restoring the level of *rag1* expression. Injection of 400 pg rescue mRNA restores significant *rag1* expression, as compared to *vegfc* MO treated embryos. Black arrow highlights area of *rag1* staining in *vegfc* morphant. (C) Percentage of total embryos scored, classified as having low or normal *rag1* expression (uninjected vs *vegfc* MO, $p=1.0x10^{-5}$; *vegfc* MO vs *vegfc* MO + 200pg mRNA, p=0.05393; *vegfc* MO vs *vegfc* MO + 400pg mRNA, p=0.0013). (D) *vegfc* crispants show decreased *rag1* expression in the thymus at

5 dpf. Injection of 400 pg rescue restores significant *rag1* expression, as compared to *vegfc* crispant treated embryos. Black arrow highlights area of *rag1* staining in *vegfc* crispant. (E) Quantification of the area of *rag1* expression: Cas9 control vs *vegfc* crispant, ****p<0.0001; *vegfc* crispant vs *vegfc* crispant + 400pg rescue mRNA, ****p<0.0001; Cas9 control vs *vegfc* crispant + 400pg rescue mRNA, not significant. (F) *vegfc* morphants show increased *cmyb* expression compared to control MO. Co-injection of *vegfc* MO and 400 pg rescue mRNA restores *cmyb* expression to control levels. In contrast, co-injection of *vegfc* MO and 400 pg control mRNA does not restore *cmyb* expression. (G) Quantification of *cmyb*$^{+}$ cells in the CHT: control MO vs *vegfc* MO, ****p<0.0001; *vegfc* MO vs *vegfc* MO + 400pg rescue mRNA, ***p=0.0002; *vegfc* MO vs *vegfc* MO + 400pg control mRNA, not significant; control MO vs *vegfc* MO + 400pg rescue mRNA, not significant. (H) Overexpression of *vegfc* in a *cd41:gfp;flk:mCherry* background using MO-resistant mRNA. (I) Quantification of *cd41*$^{+}$ cells in the CHT at 72 hpf, p=0.8863. Scale bar: (H) 50 μm. Error bars show mean ± SEM.

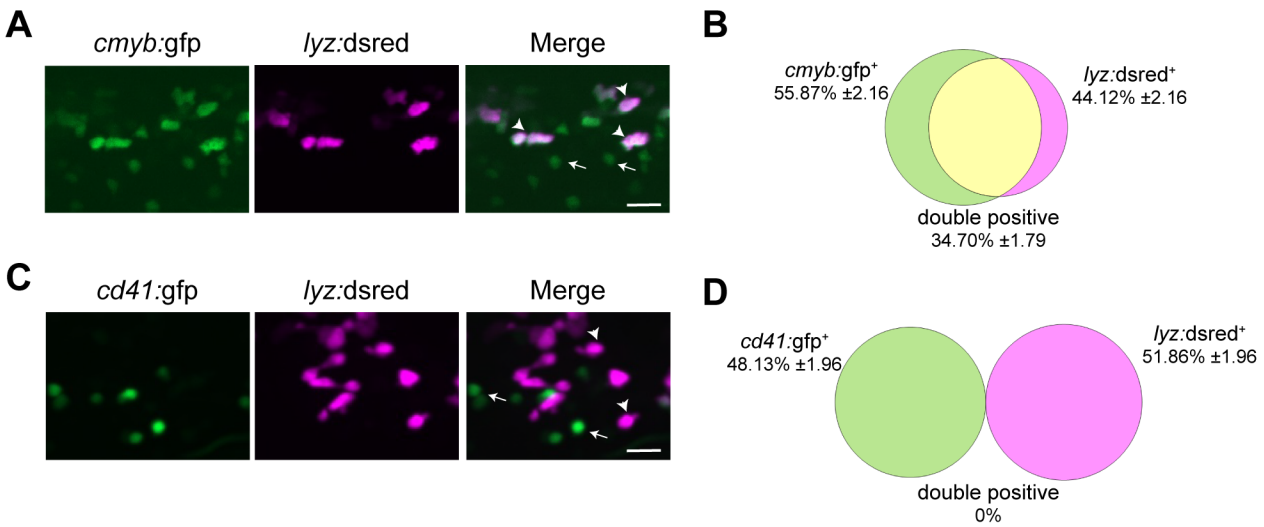

Fig. S9. *cmyb:gfp* marks myeloid cells in addition to HSPCs but *cd41:gfp* does not.

(A) A large number of *cmyb:gfp*+ cells co-localize with neutrophil marker *lyz:DsRed2*$^{+}$ cells at 72 hpf. Arrowheads indicate cells positive for *cmyb:gfp* and *lyz:DsRed2*, arrows indicate cells positive for *cmyb,* but not *lyz*. (B) Quantification of the percentage of cells positive for *cmyb:gfp*, *lyz:DsRed2* or both. N= 10 embryos. (C) There we no signs of co-localization between *cd41:gfp*+ cells and *lyz:DsRed2*+ cells at 72 hpf. Arrowheads indicate cells positive for *lyz:DsRed2*, arrows indicate cells positive for *cd41:gfp*. (D) Quantification of the percentage of cells positive for *cd41:gfp*, *lyz:DsRed2* or both. N = 8 embryos. Scale bars: 20 μm.

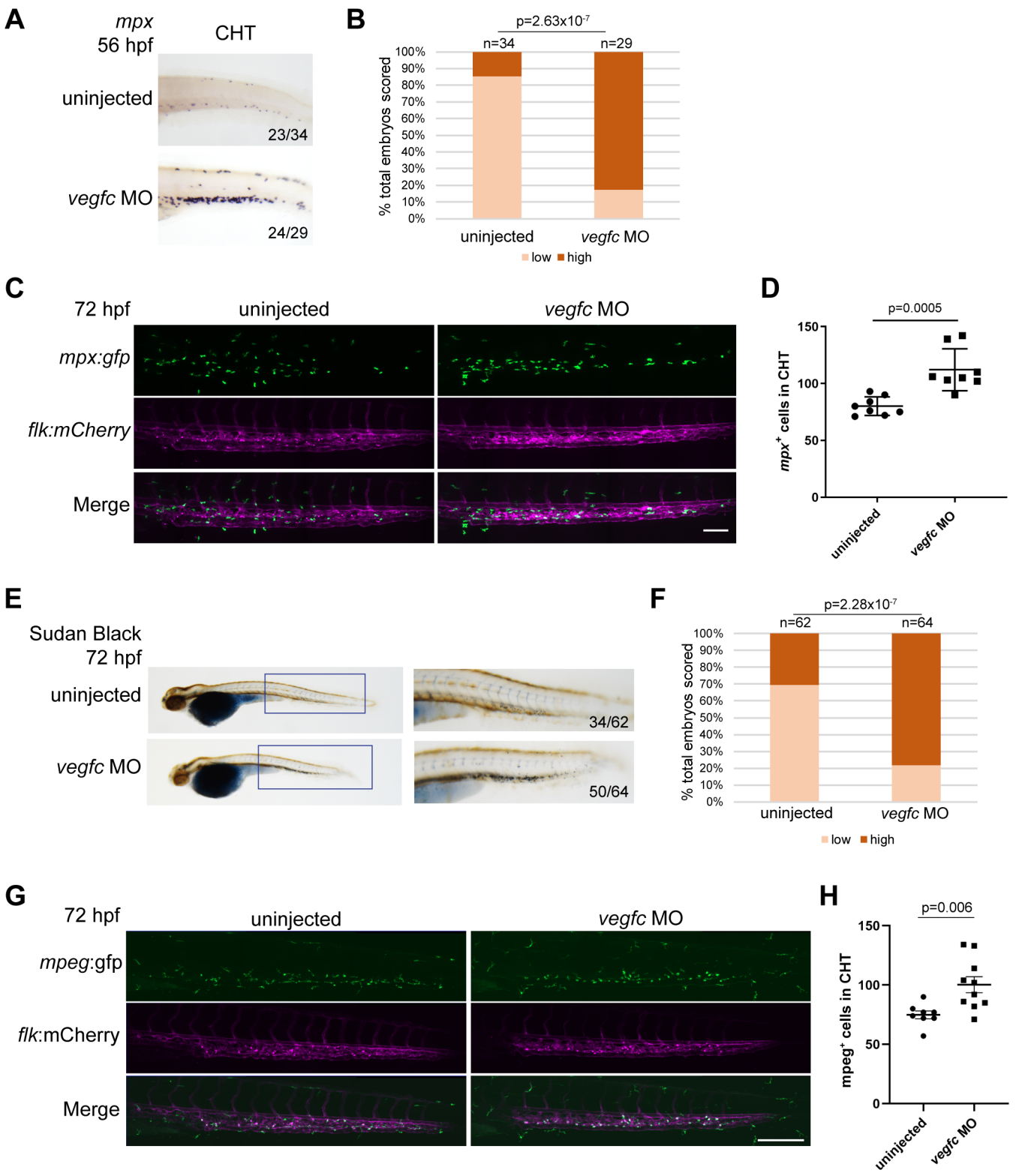

Fig. S10. Neutrophil and macrophage numbers are increased in the CHT of *vegfc* morphant embryos. A) *vegfc* loss-of-function increases the percentage of embryos with high *mpx* expression in the CHT region at 56 hpf. (B) Percentage of total embryos scored classified as having low or high *mpx* expression, $p=2.63x10^{-7}$. (C) *vegfc* loss-of-function increases the number of *mpx:gfp*+ cells in the CHT at 56 hpf. (D) Quantification of *mpx:gfp*+ cells within the CHT, p=0.0005. (E) *vegfc* morphant embryos have increased neutrophils as shown by Sudan black staining at 72 hpf. (F) Percentage of embryos scored classified as having low or high levels of Sudan black staining, $p=2.28x10^{-7}$. (G) *vegfc* loss-of-function embryos show increased numbers of macrophages in the CHT as shown by *mpeg:gfp*+ cells at 72 hpf. (H) Quantification of the number of *mpeg:gfp*+ cells within the CHT, p=0.006. Scale bars: (C): 50 ; (G): 100 μm. Error bars show mean ± SEM.

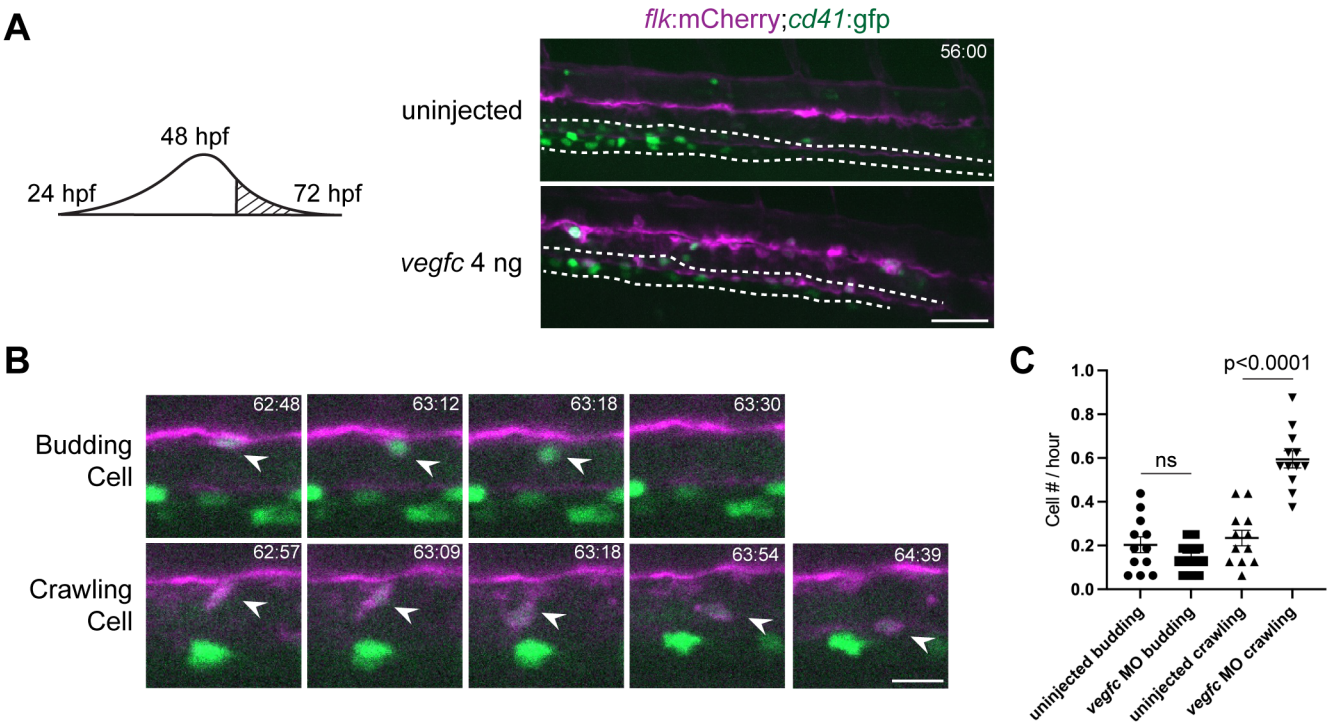

Fig. S11. Late-stage hemogenic endothelium gives rise to increased crawling myeloid-like cells in *vegfc* morphant embryos.

(A) A schematic showing the time-frame imaged falls past the peak of HSPC emergence form the DA. Single frames of time-lapse (hours post fertilization:minutes) showing the overall difference in DA morphology between uninjected controls (top panel) and *vegfc* morphants (bottom panel). The dotted line outlines the pronephric tubules (B) 4 frames selected from a control time-lapse movie between 56-72 depicting HSPC budding. 5 frames selected from *vegfc* morphant time-lapse movie depicting HSPC crawling. White arrowheads indicate the cell of interest. (C) Quantification of *flk:mCherry+/cd41:gfp+* cell behavior within the DA, p<0.0001. The total number of events observed are divided by the duration of the experiment (16 hours) to give the number of events per hour. The data shown is combined from two independent experiments with a total of n=12 uninjected and n=12 vegfc MO embryos. (D) vegfc loss-of-function increases the percentage of embryos displaying high *mpx* expression in the DA region at 56 hpf. (E) Percentage of embryos scored classified as having *mpx* expression in the DA or not, $p=2.65x10^{-5}$. Scale bar: (A) 40 μm; (B) 10 μm. Error bars show mean ± SEM.

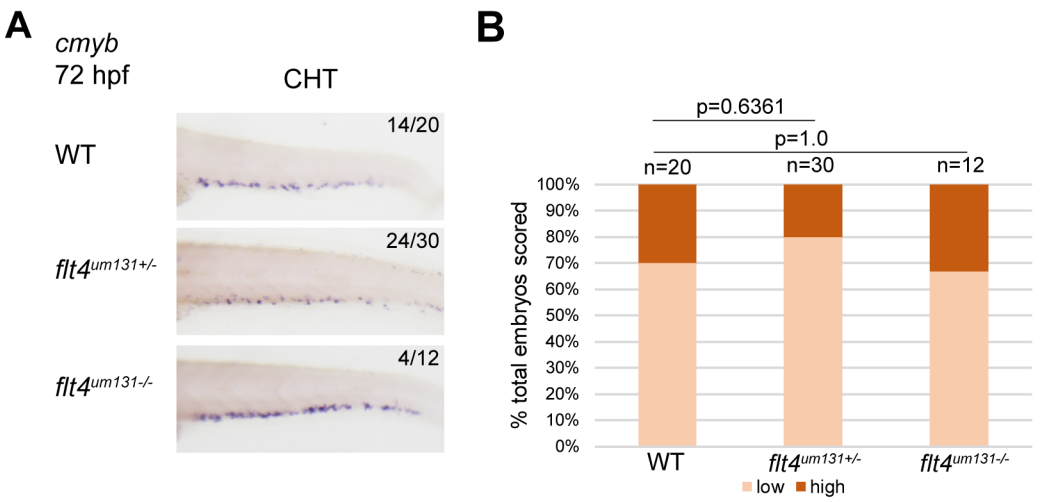

Fig. S12. *flt4/vegfr3* mutants do not have a significant change in *cmyb* expression in the CHT at 72 hpf. Compared to *vegfc*$^{um18-/-}$ mutant embryos that have increased *cmyb* expression in the CHT at 72 hpf (see Fig. 2G,H), (A) *flt4*$^{um131+/-}$ and *flt4*$^{um131-/-}$ mutant embryos show no change in *cmyb* expression in the CHT at 72 hpf when compared to WT. (B) Percentage of total embryos scored for level of *cmyb* expression. WT vs *flt4*$^{um131+/-}$ (p=0.6361) and WT vs *flt4*$^{um131-/-}$ (p=1.0).

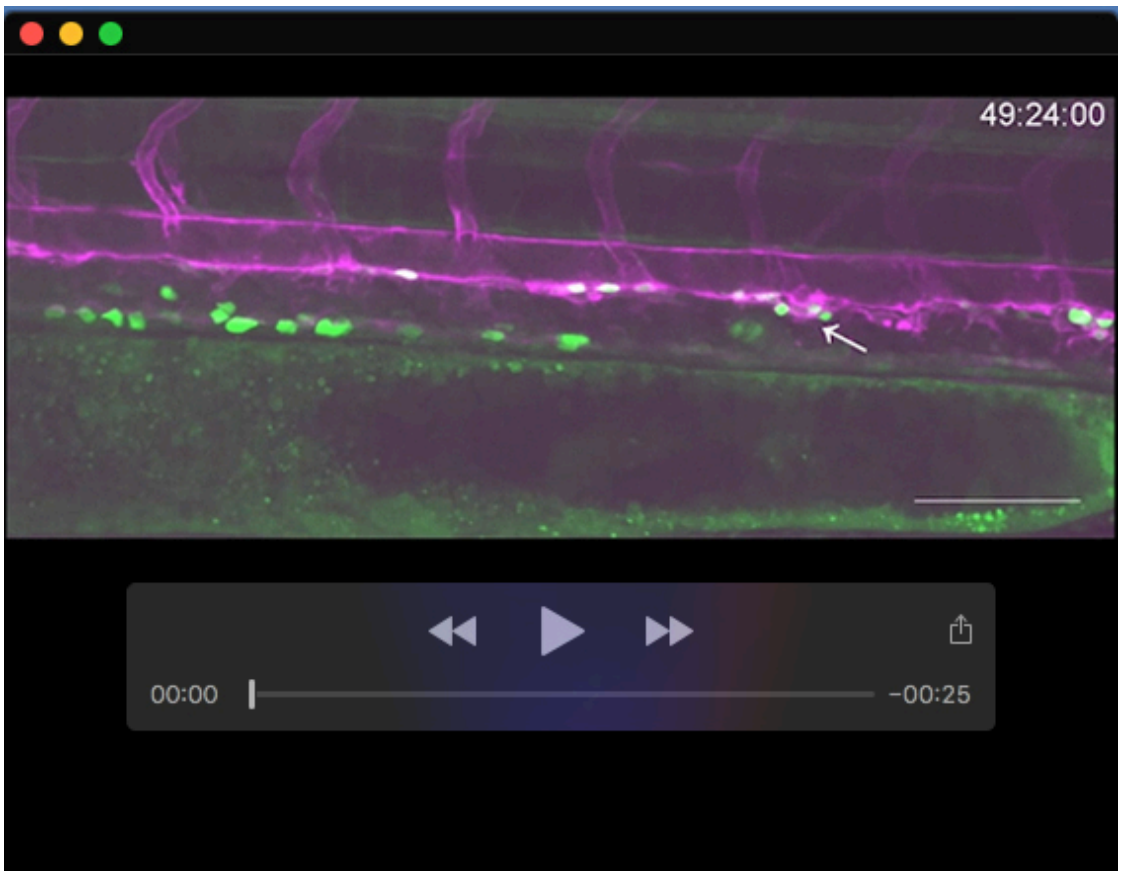

Movie 1. Control HSPC emergence from the DA.

Time-lapse imaging of *cd41:gfp* (HSPCs) and *flk:mCherry* (ECs) control embryos from 48-52 hpf. Arrows indicate cells that are undergoing EHT. Corresponds to Figure 2.

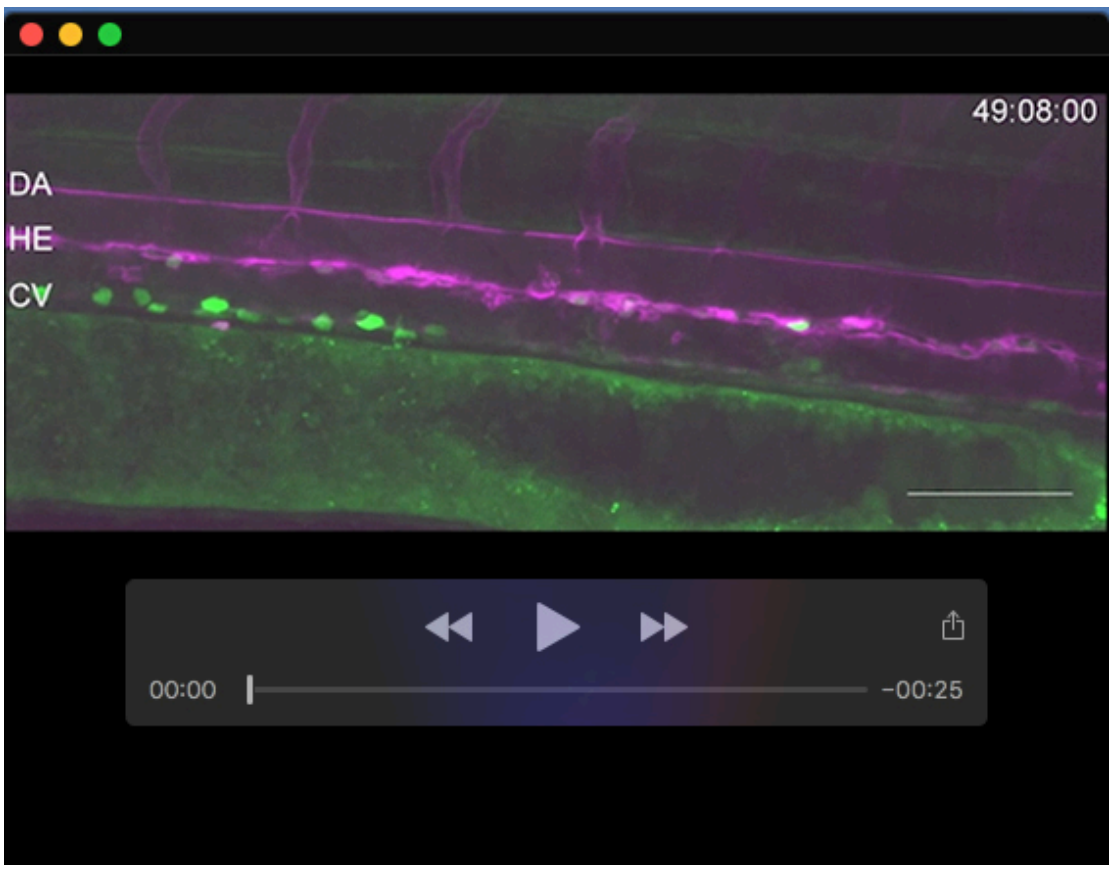

Movie 2. *vegfc* loss-of-function HSPC emergence from the DA.

Time-lapse imaging of *cd41:gfp* (HSPCs) and *flk:mCherry* (ECs) *vegfc* loss-of-function embryos from 48-52 hpf. Arrows indicate cells are unable to complete EHT. Corresponds to Figure 2.

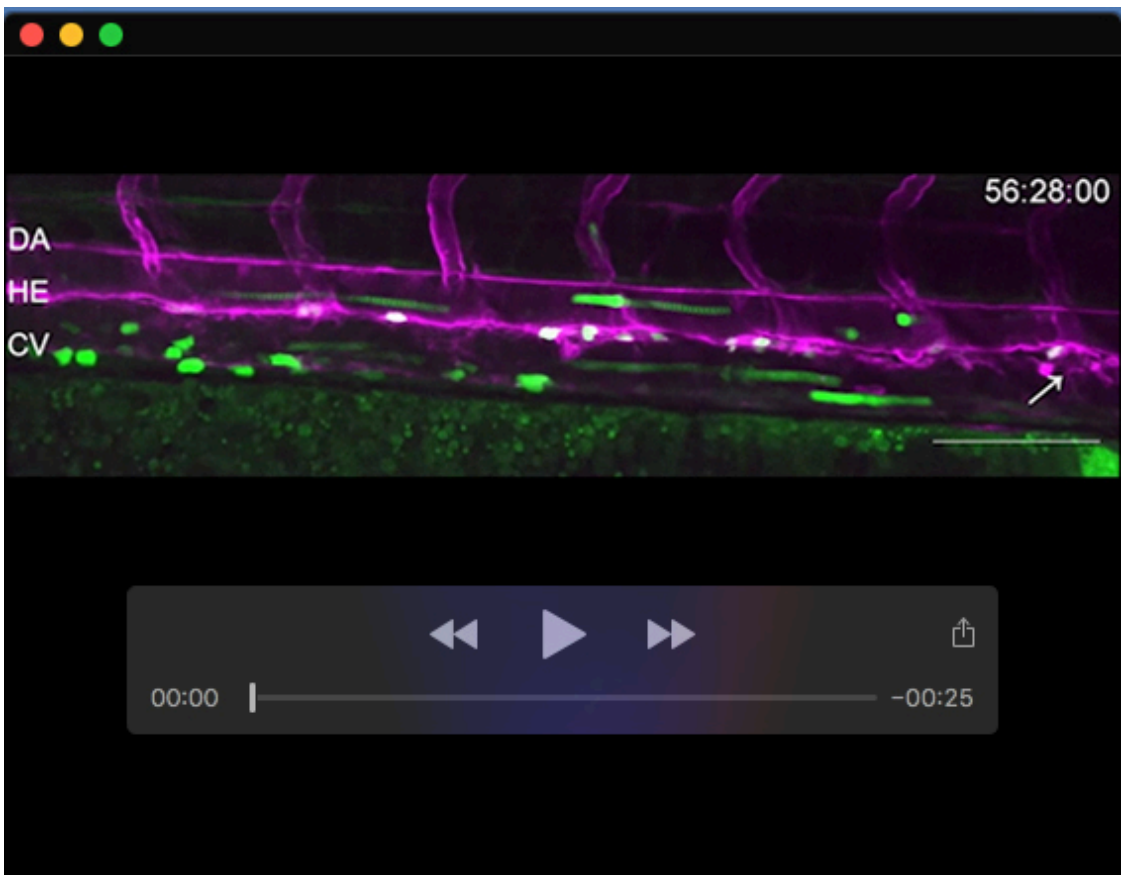

Movie 3. Control HSPC emergence from late-stage DA.

Time-lapse imaging of *cd41:gfp* (HSPCs) and *flk:mCherry* (ECs) control embryos from 56-72 hpf. Arrows indicate cells that are undergoing EHT. Corresponds to Figure 5A-C.

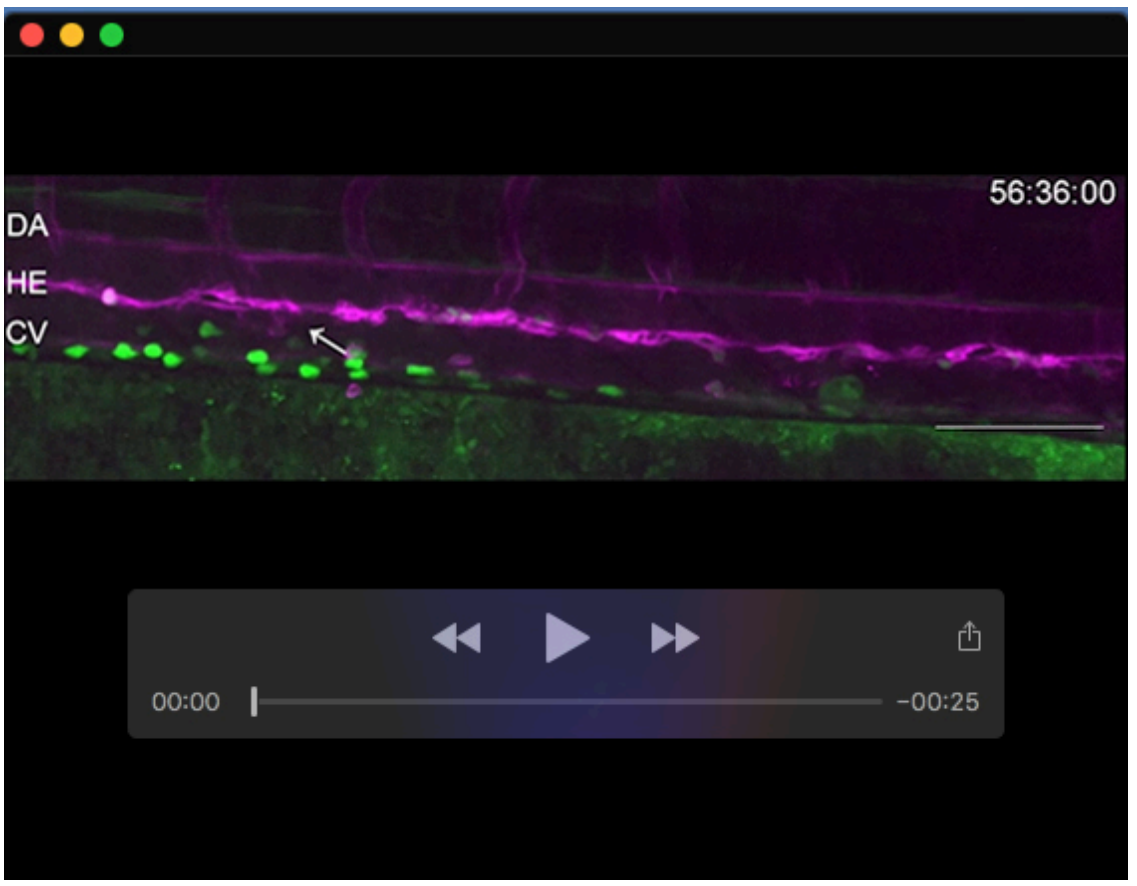

Movie 4. *vegfc* loss-of-function HSPC emergence from late-stage DA.

Time-lapse imaging of *cd41:gfp* (HSPCs) and *flk:mCherry* (ECs) *vegfc* loss-of-function crispant embryos from 56-72 hpf. Arrows indicate cells displaying crawling behavior. Corresponds to Figure 5A-C.

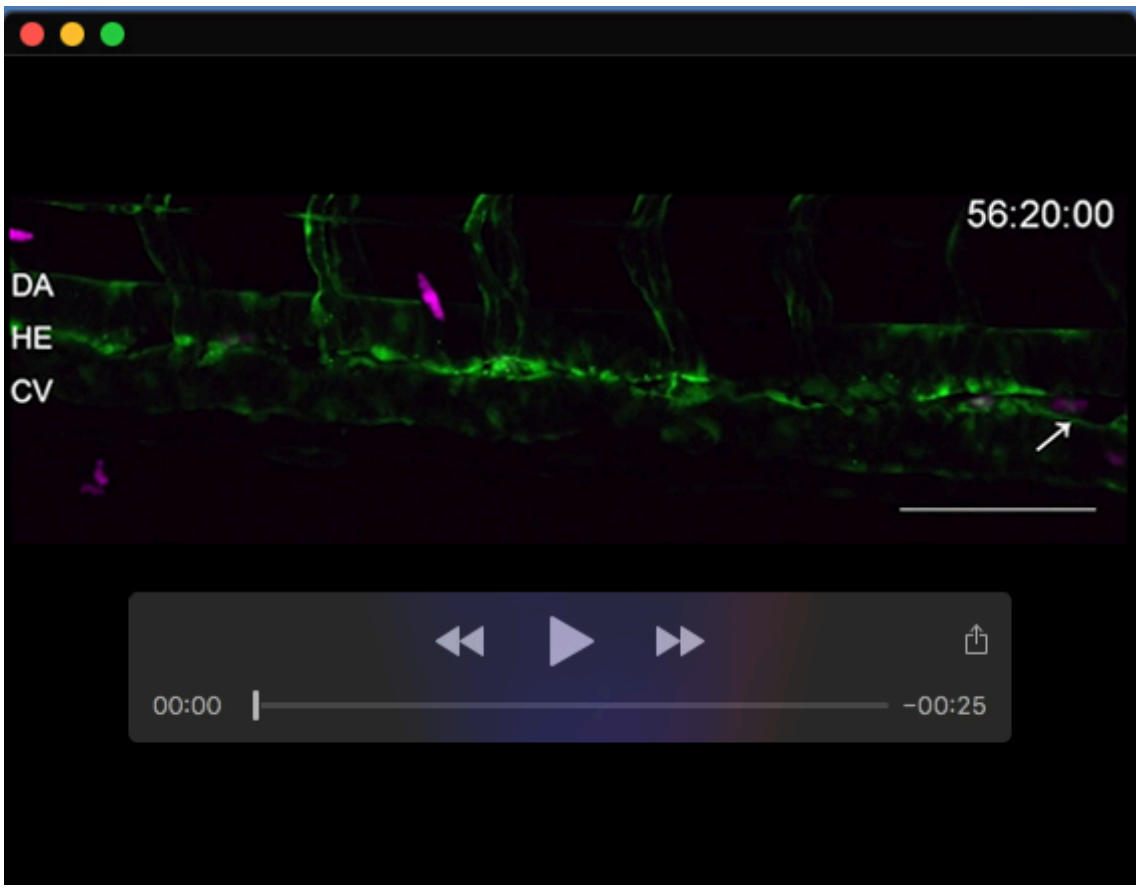

Movie 5. *lyz:DsRed2*$^{+}$ cells in control embryo late-stage DA.

Time-lapse imaging of *flk*:*gfp* (ECs) and *lyz:DsRed2* (myeloid) control embryos from 56-72 hpf. Arrows indicate *lyz:DsRed2*+ cells that reside in the DA and display crawling behavior. Corresponds to Figure 6D,E.

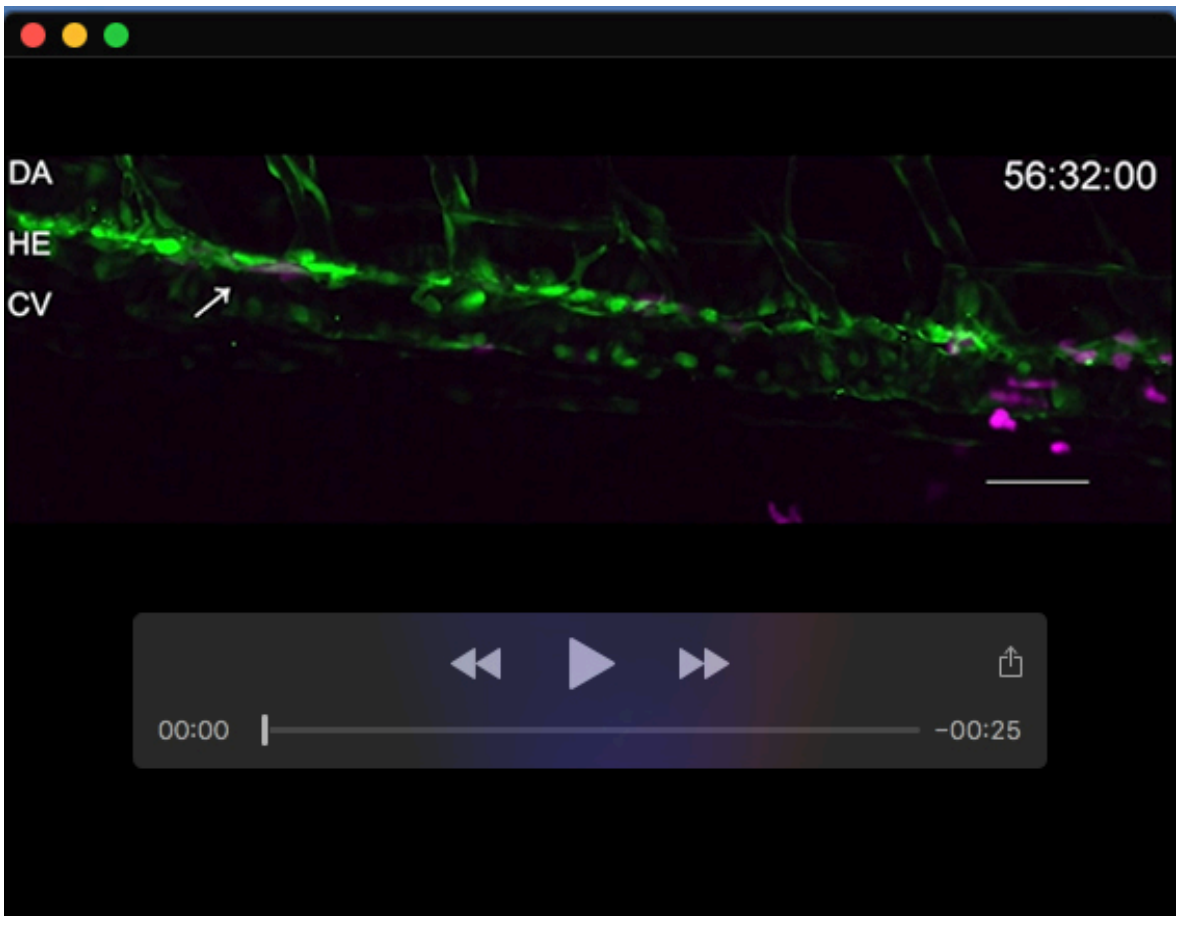

Movie 6. *lyz:DsRed2*+ cells in *vegfc* loss-of-function embryo late-stage DA.

Time-lapse imaging of *flk:gfp* (ECs) and *lyz:DsRed2* (myeloid) *vegfc* loss-of-function embryos from 56-72 hpf. Arrows indicate *lyz:DsRed2*+ cells that reside in the DA and display crawling behavior. Corresponds to Figure 6D,E.

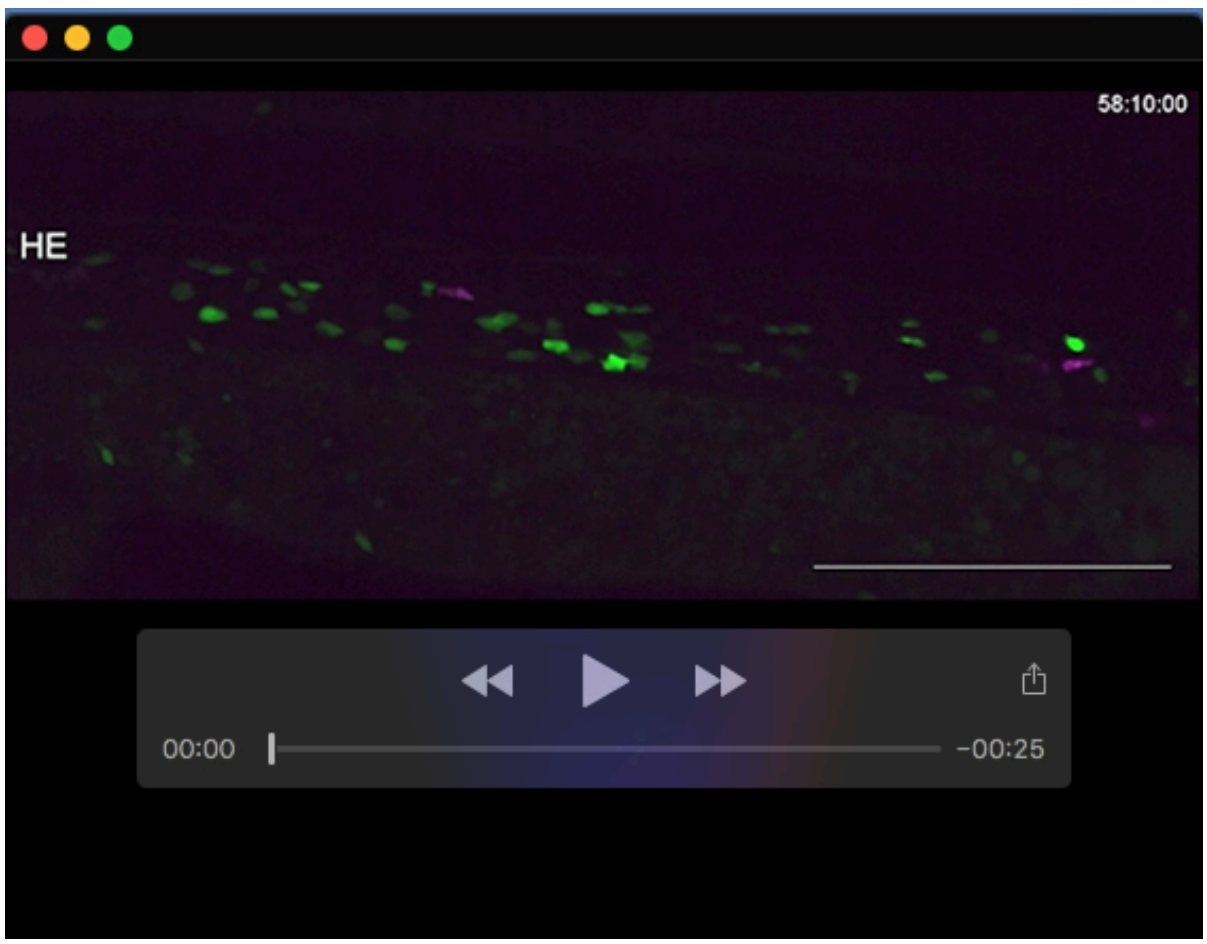

Movie 7. *lyz:DsRed2+/cd41:gfp+* cells in control embryo late-stage DA.

Time-lapse imaging of *cd41:gfp* (HSPCs) and *lyz:DsRed2* (myeloid) control embryos from 56-66 hpf. Corresponds to Figure 6F,G.

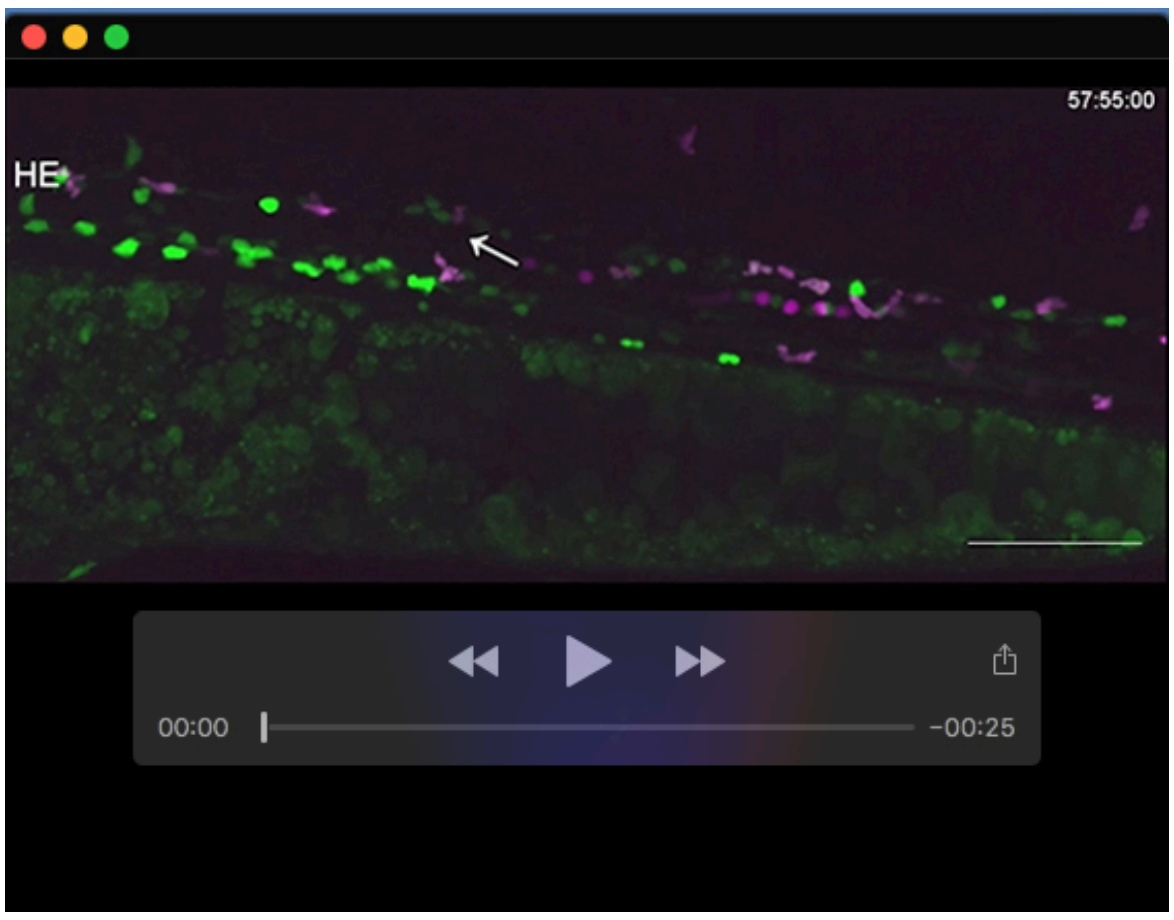

Movie 8. *lyz:DsRed2+/cd41:gfp+* cells in *vegfc* loss-of-function embryo late-stage DA.

Time-lapse imaging of *cd41:gfp* (HSPCs) and *lyz:DsRed2* (myeloid) *vegfc* loss-of-function embryos from 56-66 hpf. Arrows indicate *lyz:DsRed2+*/*cd41:gfp+* cells that reside in the DA and display crawling behavior. Corresponds to Figure 6F,G.

Supplementary References

BURGER, A., LINDSAY, H., FELKER, A., HESS, C., ANDERS, C., CHIAVACCI, E., ZAUGG, J., WEBER, L. M., CATENA, R., JINEK, M., ROBINSON, M. D. & MOSIMANN, C. 2016. Maximizing mutagenesis with solubilized CRISPR-Cas9 ribonucleoprotein complexes. *Development (Cambridge, England),* 143**,** 2025-2037.

CLEMENT, K., REES, H., CANVER, M. C., GEHRKE, J. M., FAROUNI, R., HSU, J. Y., COLE, M. A., LIU, D. R., JOUNG, J. K., BAUER, D. E. & PINELLO, L. 2019. CRISPResso2 provides accurate and rapid genome editing sequence analysis. *Nat Biotechnol,* 37**,** 224-226.

GAZIT, R., GARRISON, B. S., RAO, T. N., SHAY, T., COSTELLO, J., ERICSON, J., KIM, F., COLLINS, J. J., REGEV, A., WAGERS, A. J., ROSSI, D. J. & IMMUNOLOGICAL GENOME PROJECT, C. 2013. Transcriptome analysis identifies regulators of hematopoietic stem and progenitor cells. *Stem Cell Reports,* 1**,** 266-80.

SEITA, J., SAHOO, D., ROSSI, D. J., BHATTACHARYA, D., SERWOLD, T., INLAY, M. A., EHRLICH, L. I., FATHMAN, J. W., DILL, D. L. & WEISSMAN, I. L. 2012. Gene Expression Commons: an open platform for absolute gene expression profiling. *PLoS One,* 7**,** e40321.

ZHU, Q., GAO, P., TOBER, J., BENNETT, L., CHEN, C., UZUN, Y., LI, Y., HOWELL, E. D., MUMAU, M., YU, W., HE, B., SPECK, N. A. & TAN, K. 2020. Developmental trajectory of prehematopoietic stem cell formation from endothelium. *Blood,* 136**,** 845-856.